The deglacial history of 79N glacier and the Northeast Greenland Ice Stream

David H. Roberts [a,*], Timothy P. Lane [b], Richard S. Jones [c], Michael J. Bentley [a], Christopher M. Darvill [d], Angel Rodes [e], James A. Smith [f], Stewart S.R. Jamieson [a], Brice R. Rea [g], Derek Fabel [h], Delia Gheorghiu [h], Allan Davidson [h], Colm Ó Cofaigh [a], Jerry M. Lloyd [a], S. Louise Callard [i], Angelika Humbert [j]

[a] Department of Geography, Durham University, South Road, Durham, DH1 3LE, United Kingdom
[b] School of Biological and Environmental Sciences, Liverpool John Moores University, Liverpool, L3 3AF, United Kingdom
[c] School of Earth Atmosphere and Environment, Monash University, Wellington Road, Clayton, VIC, 3800, Australia
[d] Department of Geography, The University of Manchester, Oxford Road, Manchester, M13 9PL, United Kingdom
[e] Department of Geography, Universidade de Santiago de Compostela, Galicia, Spain
[f] British Antarctic Survey, High Cross, Madingley Road, Cambridge, CB3 0ET, United Kingdom
[g] Geography and Environment, School of Geosciences, University of Aberdeen, Elphinstone Road, Aberdeen, AB24 UF, United Kingdom
[h] NERC NEIF-CN (formerly CIAF), Scottish Universities Environmental Research Centre, East Kilbride, G75 0QF, United Kingdom
[i] School of Geography, Politics and Sociology, Newcastle University, Newcastle Upon Tyne, NE1 7RU, United Kingdom
[j] Alfred-Wegener-Institut, Helmholtz Zentrum für Polar- und Meeresforschung, Bremerhaven, Germany

ARTICLE INFO

ABSTRACT

The Northeast Greenland Ice Stream (NEGIS) is the main artery for ice discharge from the northeast sector of the Greenland Ice Sheet (GrIS) to the North Atlantic. Understanding the past, present and future stability of the NEGIS with respect to atmospheric and oceanic forcing is of global importance as it drains around 17% of the GrIS and has a sea-level equivalent of 1.6 m. This paper reconstructs the deglacial and Holocene history of Nioghalvfjerdsbræ (or 79N Glacier); a major outlet of the NEGIS.

At high elevation (>900 m asl) autochthonous blockfield, a lack of glacially moulded bedrock and pre LGM exposure ages point to a complex exposure/burial history extending back over half a million years. However, post Marine Isotope Stage 12, enhanced glacial erosion led to fjord incision and plateaux abandonment. Between 900 and 600 m asl the terrain is largely unmodified by glacial scour but post LGM erratics indicate the advection of cold-based ice through the fjord. In contrast, below ~600 m asl Nioghalvfjerdsfjorden exhibits a geomorphological signal indicative of a warm-based ice stream operating during the last glacial cycle. Dated ice marginal landforms and terrain along the fjord walls show initial thinning rates were slow between ~23 and 10 ka, but post-10 ka it is evident that Nioghalvfjerdsfjorden deglaciated extremely quickly with complete fjord deglaciation below ~500 m asl between 10.0 and 8.5 ka.

Both increasing air and ocean temperatures were pivotal in driving surface lowering and submarine melt during deglaciation, but the final withdrawal of ice through Nioghalvfjerdsfjorden was facilitated by the action of marine ice sheet instability. Our estimates show that thinning and retreat rates reached a maximum of 5.29 ma^{-1} and 613 ma^{-1}, respectively, as the ice margin withdrew westwards. This would place the Early Holocene disintegration of this outlet of the NEGIS at the upper bounds of contemporary thinning and retreat rates seen both in Greenland and Antarctica. Combined with recent evidence of ice stream shutdown during the Holocene, as well as predictions of changing ice flow dynamics within downstream sections of the NEGIS catchment, this suggests that significant re-organisation of the terminal zone of the ice stream is imminent over the next century.

1. Introduction

Over the last two decades the incursion of warm Atlantic Water as well as increased air temperatures and sea-ice loss, have been linked to the recession and thinning of marine terminating glaciers in Greenland (Straneo and Heimbach, 2013; Schaffer et al., 2020). However, despite our improved understanding of the mechanisms that drive glacier change (Shepherd et al., 2020), the short time span of observations in polar regions provide only a limited time series with which to understand and model the complex and non-linear response of marine-terminating ice streams to ocean/atmospheric forcing. This restricts our ability to understand and project how ice sheets will change over the coming centuries (Seroussi et al., 2013; Goelzer et al., 2020). What we fundamentally lack is decadal - millennial scale input data to calibrate, verify and benchmark the sensitivity of predictive models. One solution is to identify patterns of former rapid ice margin evolution where the key forcing mechanisms that influence ice sheet stability can also be simultaneously reconstructed so their relative importance can be determined.

This study reconstructs the past dynamics of the Northeast Greenland Ice Stream (NEGIS); the main artery for ice discharge from the NE sector of the Greenland Ice Sheet (GrIS) to the North Atlantic (Fig. 1). NEGIS is the largest ice stream in Greenland (Fahnestock et al., 1993; Joughin et al., 2010) and branches into three outlet glaciers Nioghalvfjerdsbraeæ (79N Glacier), Zachariaeæ isstrøm (ZI) and Storstrømmen Glacier (SG) (Fig. 1). Both 79N Glacier and ZI are fast flowing ice streams buttressed by ice shelves, while SG terminates in a slow flowing, low gradient ice plain. Understanding the behaviour of NEGIS and its future stability is important as it drains around 17% of the GrIS, has a sea-level equivalent of 1.6 m (Fahnestock et al., 1993, Joughin et al., 2010; Aschwanden et al., 2019; Krieger et al., 2019) and is directly connected to the North Atlantic via its marine termini ZI and 79N Glacier. Prior to the 2000's both ZI and 79N Glacier showed little response to atmospheric and ocean warming, but post 2006 these glaciers have undergone flow acceleration, retreat and thinning. ZI in particular has undergone dramatic changes with marked speed-up and ice shelf break-up in 2012 (Khan et al., 2014; Mouginot et al., 2015).

Choi et al. (2017) project that ZI will be unstable over the coming decades with high submarine melt rates and bathymetric over-deepening likely to increase retreat rates. If submarine melt rates exceed 6 m per day, ZI may retreat further, potentially contributing up to 16.2 mm to global sea level rise by 2100 (Choi et al., 2017; Larsen
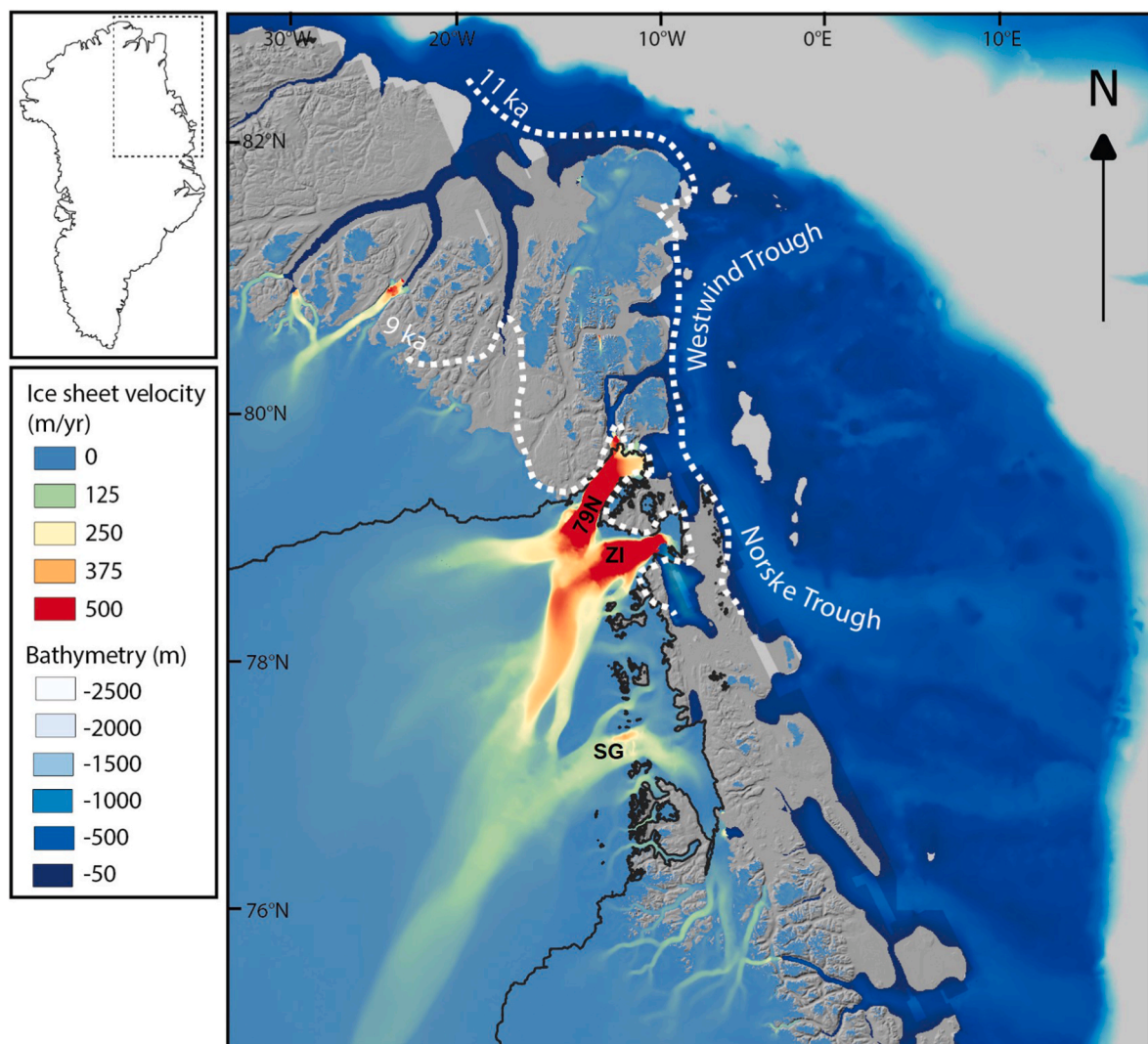

Fig. 1. The NE sector of the Greenland Ice Sheet (GrIS) with the NEGIS flowing from the ice divide northeastwards. The ice stream currently terminates in the 79 N ice shelf, the remnant of the Zachariaeæ isstrøm ice shelf and the Storstrømmen glacier further south. At the LGM the former NEGIS terminated offshore at the continental shelf edge via the Westwind and Norske troughs. The dotted white lines represent the 11ka and 9ka retreat positions of the GrIS (Larsen et al., 2018; Smith et al., 2023). Ice sheet velocity generated using auto-RIFT (Gardner et al., 2018) and provided by the NASA MEaSUREs ITS_LIVE project (Gardner et al., 2019). Overlain on the ArcticDEM with IBCAO bathymetry (Jakobsson et al., 2020). Figure generated using QGreenland (Moon et al., 2021).

et al., 2018). In contrast, the adjacent outlet of 79N Glacier and its ice shelf have been relatively stable post 2012, in part due to a bathymetric high adjacent to the present grounding line. However, recent observations suggest submarine melt rates are likely to increase as Atlantic Water continues to ingress the 79N Glacier sub-shelf cavity, potentially triggering ice shelf disintegration (Mayer et al., 2018; Wilson and Straneo, 2015; Schaffer et al., 2020; An et al., 2021; Bentley et al., 2023; Millan et al., 2023; Zeising et al., 2023). Khan et al. (2022), have identified significant and ongoing surface thinning (2011–2021) at both the ZI and 79N Glacier margins (1.5–3.5 ma^{-1}) which has propagated inland. Such changes will influence decadal to millennial scale ice flux of ice through the NEGIS system.

Importantly, during the Holocene Thermal Maximum (HTM; 8.0–5.0 ka BP), the 79N ice shelf retreated over 100 km westward of the present day coast (Bennike and Weidick, 2001; Larsen et al., 2018; Smith et al., 2023). This was a period when air and sub-surface ocean temperatures were higher than those predicted for 2100AD (Klug et al., 2009; Werner et al., 2016), and yet, rates of grounding line retreat, ice stream thinning and ice shelf loss remain poorly constrained. In addition, it is now evident from ice radar data that upstream parts of the NEGIS catchment underwent phases of ice flow switching and partial shutdown at some point in the Holocene (Franke et al., 2022). Such an event in the coming decades could significantly affect ice sheet-wide mass balance and ice flux from the NEGIS catchment to the North Atlantic.

This paper seeks to establish the timing of ice stream and ice shelf retreat and thinning through the Nioghalvfjerdsfjorden during the end of the Last Glacial Maximum (LGM; 26–19.5 ka BP) and into the Holocene. It establishes rates of palaeo-ice stream thinning/retreat and tests the hypothesis that the 79N Glacier grounding line and ice shelf collapsed rapidly during the Early Holocene. These findings are considered against the key environmental variables influencing ice sheet mass balance during the end of the LGM and into the Holocene and are contextualised against recent observations from major ice stream catchments in Greenland and Antarctica.

1.1. NEGIS – past behaviour

The known deglacial history of NEGIS demonstrates sustained and enhanced retreat in response to periods of warming. Prior to the LGM, Larsen et al. (2018) provide evidence from SG for ice retreat and marine incursion up to 40 km inland between 37.0 and 28.4 ka, while evidence from Lambert Land and ZI suggests ice had retreated 20–40 km west of the present ice margin from ~41.0 ka until after 26 ka. Larsen et al. (2018) link this recession to higher boreal summer insolation with relatively mild summers and low snow accumulation rates during MIS 3. The LGM in NE Greenland is constrained to 26–20 ka and coincided with low obliquity, a low precession index, low summer insolation (JJA) and low summer air temperatures (Nørgaard-Pedersen et al., 2008; Larsen et al., 2018). Following the LGM, ice sheet retreat across the continental shelf was well under way by 15.0–14.0 ka (Stein et al., 1996). Davies et al. (2022) report ice retreat across the inner NE Greenland continental shelf between 13.4 and 12.5 ka BP, driven by an influx of Atlantic Water.
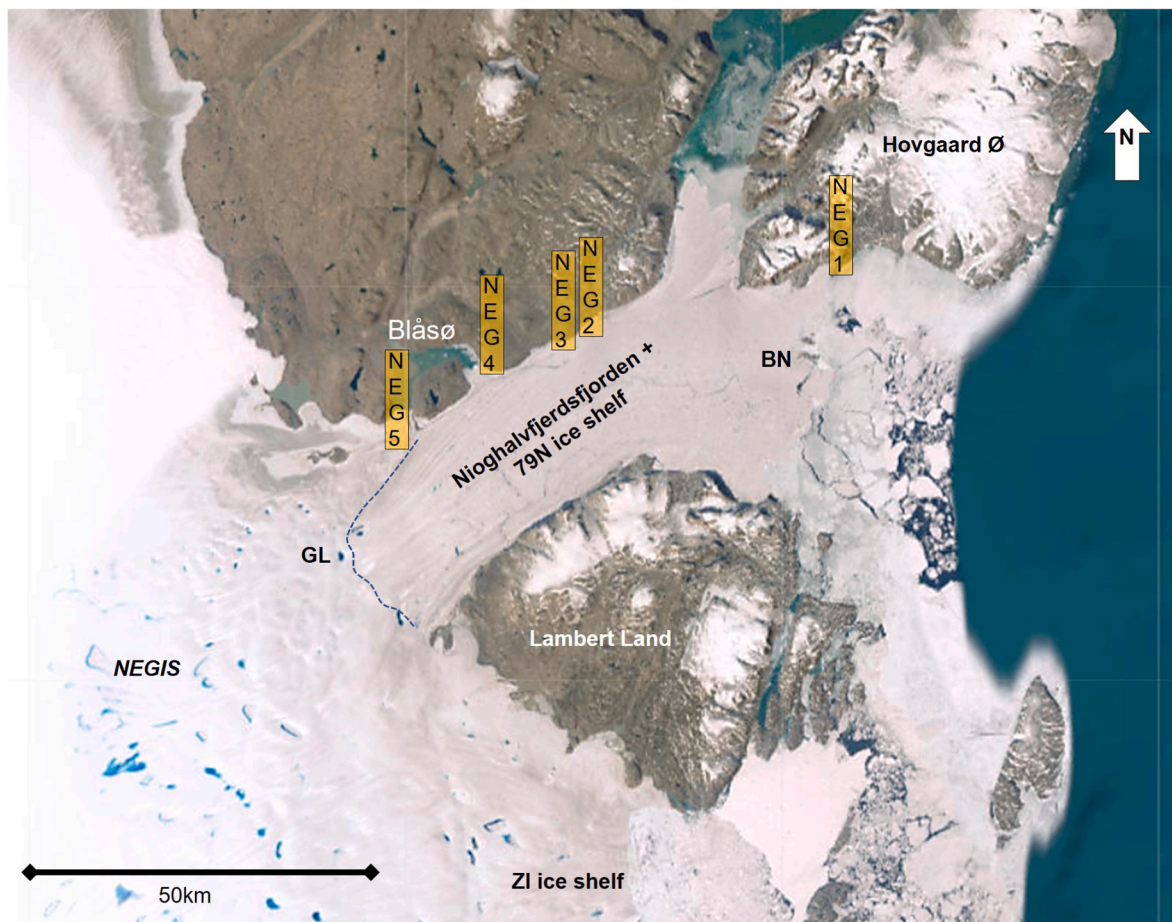

Fig. 2. Nioghalvfjerdsfjorden currently harbours the 79N ice shelf which is ~75 km long. The contemporary grounding line of the ice stream is situated ~20 km west of Blåsø, and the ice shelf margin terminates on a chain of bedrock pinning points (Bloch Nunatakker; BN); south of Hovgaard Ø. At the grounding line (GL) the trough floor reaches ~ 900 m bsl (Morlighem et al., 2017). Terrain adjacent to 79N reaches an elevation of 1200 m asl with high elevation plateaux harbouring local ice caps and autochthonous blockfield. Allochthonous blockfield and erratics occur between 900 and 600 m asl along the steep fjord walls. Below 600 m asl the terrain is ice scoured. NEG1-NEG5 mark locations of cosmogenic sampling transects.

Arndt et al. (2017) hypothesise a possible mid-shelf Younger Dryas re-advance although this lacks geochronological support.

Ice recession to the outer coast is well constrained by [10]Be exposure ages around 11.7–11.3 ka, with ice stepping back to the inner coast and several pinning points between ~10.0 and 9.0 ka (Larsen et al., 2018). This period of ice sheet retreat to the coast correlates with peak obliquity and precession and large increases in air and sub-surface ocean temperatures. At the eastern end of Nioghalvfjerdsfjorden, Syring et al. (2020) provide clear evidence for ice shelf absence and sea-ice presence in front of 79N as the grounding line became pinned on the island chain associated with Bloch Nunatakker (Fig. 2). Post 9.1 ka, radiocarbon dates on driftwood and whalebones associated with shorelines along Nioghalvfjerdsfjorden and around Blåsø (Bennike and Weidick, 2001), as well as marine microfossils from cores recovered from the lake at Blåsø (Smith et al., 2023), indicate open water conditions in Nioghalvfjerdsfjorden between 8.5 and 4.4 ka. [10]Be exposure ages were also used to infer that the NEGIS grounding line was ~20–70 km farther inland than present in the period ~7.8–1.2 ka (Larsen et al., 2018).

The timing of this Early to Mid-Holocene retreat in Nioghalvfjerdsfjorden broadly correlates with the HTM in Greenland (Dahl-Jensen et al., 1998), rapid sea-ice loss on the East Greenland shelf at ~8 cal. Ka BP and increased ocean temperatures adjacent to NEGIS (Vinther et al., 2009; Müller et al., 2012; Werner et al., 2016; Syring et al., 2020; Davies et al., 2022; Lloyd et al., 2023). However, the rate and magnitude of this Early Holocene retreat event remains poorly constrained and could have occurred on decadal/centennial timescales (cf. Choi et al., 2017). Post ~4.4 ka, Smith et al. (2023) demonstrate that Nioghalvfjerdsfjorden was re-occupied by an ice shelf which advanced and became pinned at the outer fjord. Reformation of the ice shelf coincided with decreasing atmospheric temperatures, a reduction in Atlantic Water influence, increased sea-ice cover and the presence of Polar Water on the NE Greenland continental shelf (Lloyd et al., 2023). This was part of a pan-ice sheet response to Neoglacial cooling resulting in GrIS regrowth up to the Little Ice Age (Kjær et al., 2022).

1.2. Study site

Nioghalvfjerdsfjorden is 80 km long and up to 20 km wide. At its eastern end several shallow pinning points form a chain of islands that runs north to south, but water depths increase rapidly to the west where the NEGIS grounding line terminates 900 m bsl (Morlighem et al., 2017). Mountainous terrain borders the fjord with plateau surfaces reaching 1500–2000m asl (Lane et al., 2023). The geological setting is complex (Smith et al., 2004). The western end of Hovgaard Ø is underlain by quartzites of the Palaeoproterozic Independence Fjord/Hovgaard Ø Group which are crosscut by the Midgaardsormen Dolerites. The eastern half of the island is underlain by orthogneisses as are the chain of islands guarding the mouth of the fjord associated with Bloch Nunatakker. The geology of the mid and inner fjord is dominated by the Neoproterozoic Riverdal group consisting of conglomerates, sandstones and mudstones. West of the epishelf lake at Blåsø the terrain is composed of limestones of the Odin Fjord Formation.

2. Methods

2.1. Sampling strategy

In order to constrain ice stream thinning and retreat rates for the onset of deglaciation through the Holocene a two-fold approach was adopted for the sampling of terrestrial cosmogenic nuclides (TCN). Firstly, a set of vertical transects were established at outer, mid and inner fjord locations along the northern edge of Nioghalvfjerdsfjorden (NEG1-5, Figs. 2 and 3). These covered a vertical elevation range of 1100 m and a lateral distance of 80 km from the outer coast at Hovgaard Ø to the western end of the fjord close to Blåsø and the contemporary grounding line. Secondly, TCN samples were collected from locations adjacent to the vertical transects where specific ice marginal features could be identified and mapped in relation to both ice stream and ice shelf thinning (e.g. lateral moraines; ice shelf moraines; ice contact deltas; marine limits) (Lane et al., 2023). In high-elevation blockfield terrain, samples were collected from bedrock that may have been covered by cold-based ice and analysed for both [10]Be and [26]Al concentrations to establish any complex burial/exposure histories. In ice-scoured terrain eroded by warm-based ice, samples were collected from both bedrock and erratics (in boulder-bedrock pairs where possible) and were analysed for [10]Be concentrations (Table 1). Vertical sample resolution on each transect varied between 50 and 100 m. All samples from erratics were taken from surfaces >50 cm above local ground level to avoid snow and sediment cover. Where possible, sampled surfaces were striated and polished and over 30 cm from all edges with minimum granular disintegration and lichen cover (Roberts et al., 2008).

2.2. Processing TCN samples

Sample preparation was carried out following the same procedures as described in Mendelová et al. (2020). The [10]Be/[9]Be and [26]Al/[27]Al ratios were measured and calculated on the 5 MV accelerator mass spectrometer (AMS) at SUERC (Xu et al., 2010). [10]Be concentrations are based on the [10]Be/[9]Be ratio of 2.79·x 10^{-11} for NIST SRM4325. [26]Al concentrations are based on the [26]Al/[27]Al ratio of 4.11·10^{-11} for Purdue Z92-0222. Processed blank ratios subtracted from measured ratios were
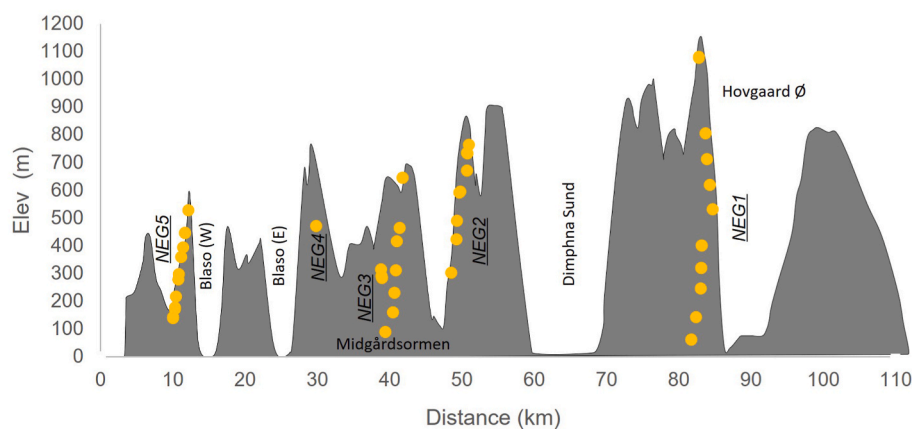

Fig. 3. A topographic long profile looking northward at the northern edge of Nioghalvfjerdsfjorden with the vertical and lateral distribution of the surface exposure ages shown from vertical transect NEG 1 in the east, through NEG 2/3/4 in the mid fjord area and NEG5 in the west (Topographic source: Google Earth Pro).

Table 1
Details for ^{10}Be and ^{26}Al samples along the northern edge of Nioghalvsfjerdfjorden.

Sample ID	Lat_DD	Long_DD	Elev (m)	Sample Type	Lithology	Thick-ness (cm)	Density (gcm^3)	Shielding factor	^{10}Be	^{26}Al
NEG101	79.743	−19.307	1081	bedrock	quartzite	4	2.65	0.9999	Yes	Yes
NEG102	79.743	−19.307	1077	bedrock	quartzite	4	2.65	0.9999	Yes	Yes
NEG104	79.731	−19.237	806	erratic	quartzite	4	2.65	0.9986	Yes	Yes
NEG105	79.740	−19.242	713	erratic	quartzite	4	2.65	0.9988	yes	Yes
NEG106	79.741	−19.224	619	bedrock	quartz	4	2.65	0.9991	Yes	
NEG109	79.738	−19.199	532	erratic	quartzite	4	2.65	0.9956	Yes	
NEG114	79.723	−19.251	401	bedrock	quartz	4	2.65	0.9998	Yes	
NEG115	79.723	−19.252	400	erratic	quartzite	4	2.65	0.9923	Yes	
NEG116	79.721	−19.253	320	erratic	quartzite	4	2.65	0.9891	Yes	
NEG117	79.721	−19.253	320	bedrock	quartz	4	2.65	0.9891	Yes	
NEG119	79.719	−19.252	246	erratic	quartzite	4	2.65	0.9928	yes	
NEG121	79.715	−19.281	142	bedrock	quartz	4	2.65	0.9968	Yes	
NEG122	79.708	−19.302	62	erratic	quartzite	4	2.65	0.9983	Yes	
NEG123	79.708	−19.302	62	bedrock	quartz	4	2.65	0.9983	yes	
NEG202	79.694	−20.950	764	bedrock	quartz	4	2.65	0.9998	Yes	yes
NEG203	79.694	−20.944	735	erratic	conglomerate	4	2.65	0.9996	Yes	
NEG204	79.693	−20.945	734	bedrock	quartz	4	2.65	0.9996	Yes	
NEG206	79.677	−20.946	671	bedrock	gneiss	4	2.65	0.9999	Yes	
NEG208	79.673	−20.942	596	bedrock	quartz	4	2.65	0.9990	Yes	
NEG209	79.673	−20.948	592	erratic	granite/gneiss	4	2.65	0.9996	Yes	
NEG211	79.671	−20.960	490	erratic	granite/gneiss	4	2.65	0.9985	Yes	
NEG212	79.669	−20.959	423	erratic	conglomeratic sandstone	4	2.65	0.9951	yes	
NEG213	79.666	−20.995	303	erratic	conglomeratic sandstone	4	2.65	0.9966	Yes	
NEG/DELTA1-01	79.667	−21.558	315	cobble	quartzite	4	2.65	0.9996	Yes	
NEG/DELTA1-03	79.666	−21.548	291	cobble	quartzite	4	2.65	0.9997	Yes	
NEG/DELTA1-03(ii)	79.666	−21.548	291	cobble	quartzite	4	2.65	0.9997	Yes	
NEG/DELTA-03 B	79.667	−21.545	284	cobble	quartzite	4	2.65	0.9997	Yes	
NEG301	79.637	−21.310	465	erratic	quartz	4	2.65	0.9999	Yes	
NEG302	79.635	−21.330	416	erratic	quartz conglomerate	4	2.65	0.9999	Yes	
NEG303	79.629	−21.322	312	erratic	sandstone	4	2.65	0.9999	Yes	
NEG305	79.625	−21.320	231	erratic	quartz	4	2.65	0.9983	Yes	
NEG306	79.623	−21.326	159	erratic	sandstone	4	2.65	0.9983	Yes	
NEG308	79.621	−21.379	89	erratic	sandstone	4	2.65	0.9994	Yes	
NEG/MOR/1	79.691	21.471	645	erratic	quartzite	4	2.65	0.9999	Yes	
NEG/MOR/2	79.691	21.471	645	erratic	quartzite	4	2.65	0.9999	Yes	
NEG405	79.607	−21.874	471	erratic	quartzite	4	2.65	0.9998	Yes	
NEG502	79.531	−22.656	529	erratic	gneiss	4	2.65	0.9999	Yes	
NEG504	79.527	−22.669	448	erratic	granite	4	2.65	0.9994	Yes	
NEG505	79.527	−22.670	446	erratic	sandstone	4	2.65	0.9997	Yes	
NEG507	79.525	−22.674	394	erratic	gneiss	4	2.65	0.9975	Yes	
NEG508	79.522	−22.679	360	erratic	granite	4	2.65	0.9993	Yes	
NEG510	79.520	−22.687	298	erratic	sandstone	4	2.65	0.9983	Yes	
NEG511	79.519	−22.688	279	erratic	sandstone	4	2.65	0.9982	Yes	
NEG513	79.518	−22.706	216	erratic	granite	4	2.65	0.9989	Yes	
NEG515	79.516	−22.705	171	erratic	granite	4	2.65	0.9986	Yes	
NEG516	79.516	−22.708	177	erratic	gneiss	4	2.65	0.9974	Yes	
NEG517	79.515	−22.718	143	erratic	quartzite	4	2.65	0.9991	Yes	
NEG518	79.515	−22.718	141	erratic	quartzite	4	2.65	0.9992	Yes	
NEG519	79.515	−22.717	139	bedrock	quartz	4	2.65	0.9996	Yes	

$6.583 \cdot 10^{-15}$ for ^{10}Be/^{9}Be (0.1–9.2% of the sample ratio) and $2.76 \cdot 10^{-15}$ for ^{26}Al/^{27}Al (0.1–1.1% of the sample ratio). The uncertainty of this correction is included in the stated uncertainties. Calculated ^{10}Be and ^{26}Al concentrations and ages are given in Table 2. Full sample details including data on quartz (g), carrier (μg ^{9}Be), sample ^{27}Al (μg) determined by ICP-OES, ^{10}Be/^{9}Be and ^{26}Al/^{27}Al for samples and procedural blanks and related uncertainties are provided in Supplementary Information (Table 5).

2.3. Calculation of TCN ages

Exposure ages and internal uncertainties were calculated using the CRONUS-Earth online calculators version 3 (http://hess.ess.washington.edu/math/; Version info: Get age: 3.0.2; muons: 1 A, alpha = 1; validate: validate_v3_input.m - 3.0; consts: 3.0.4) using the Arctic production rate of Young et al. (2013). Results using the time dependent LSDn scheme are shown (Table 2). External uncertainties are indicated in brackets. Previously published TCN ages from the region have been re-calculated using CRONUS v3 for comparative purposes.

Outliers were assessed using a three-fold approach. First, apparent

TCN (^{10}Be) ages older than 30 ka were assumed to be pre LGM and to have a nuclide concentration inherited from a previous period of exposure (Nørgaard-Pedersen et al., 2008; Larsen et al., 2018; Balco, 2020). Second, linear regression analysis was applied to each vertical transect of exposure ages, and an outlier was identified if it lay outside of the regressed thinning profile at 95% confidence (iceTEA, Jones et al., 2019). While this approach works well where a clear monotonic thinning trend exists, it is less effective if there is a change in the thinning trend or if the ages are too scattered, which is the case for several transects in our dataset. Therefore, a third approach was used based on the assumed stratigraphic relationship of the samples ages; TCN ages should get younger with decreasing elevation as each sample was progressively exposed by a lowering glacier surface profile. The stratigraphic approach identified outliers based on the age of each sample (mean and 1 st.dev.) compared to that of samples stratigraphically above/below it (code found at https://github.com/rs-jones/find-outliers-transect). Each sample was assessed in turn, running from top-to-bottom and then bottom-to-top within the transect; a sample was considered a 'likely stratigraphic outlier' if it was identified as relatively too old/young in either direction.

Table 2

^{10}Be and ^{26}Al cosmogenic surface exposure ages (LSDn) for samples along the northern edge of Nioghalvsfjerdfjorden. Samples marked * were excluded from final analyses of retreat and thinning history if they were older than 30 ka or identified as a likely stratigraphic outlier.

Sample	Accel'r ID	^{10}Be/g Qtz	^{10}Be Int. error (1 sigma) (yr)	^{10}Be ext. error (1 sigma) (yr)	^{10}Be age Cronus V3 LSDn (yr)
10Be data					
*NEG101**	*b11689*	*4394995 ± 93019*	*9909*	*20068*	*419690*
*NEG102**	*b11618*	*4987200 ± 111552*	*12335*	*23955*	*485525*
*NEG104**	*b11690*	*327520 ± 10216*	*1139*	*1796*	*36811*
NEG105	b11691	187474 ± 5966	699	1110	22947
NEG106	b11619	142083 ± 4358	556	901	18893
*NEG109**	*b11620*	*185409 ± 5320*	*756*	*1267*	*27025*
NEG114	b11621	63999 ± 2852	424	576	10427
NEG115	b11700	56430 ± 2328	324	476	9328
NEG116	b11622	56742 ± 3106	479	611	10095
NEG117	b11624	51782 ± 2320	364	502	9221
NEG119	b11692	47578 ± 2184	363	501	9232
NEG121	b11625	37358 ± 1793	313	430	7866
NEG122	b11626	36092 ± 1725	319	444	8226
NEG123	b11693	31384 ± 1760	330	429	7336
NEG202	b11627	173726 ± 5062	573	949	20150
NEG203	b11628	123789 ± 3798	432	701	14711
NEG204	b11631	91770 ± 3214	353	539	10865
*NEG206**	*b11632*	*342575 ± 9508*	*1210*	*2050*	*43790*
*NEG208**	*b11696*	*322483 ± 7764*	*1069*	*1991*	*44466*
NEG209	b11633	85748 ± 3240	387	583	11627
*NEG211**	*b11634*	*102657 ± 3630*	*499*	*765*	*15450*
NEG212	b11697	52374 ± 2288	313	446	8481
NEG213	b11635	46207 ± 1813	279	417	8289
NEG/DELTA1-01	b11663	67678 ± 2684	439	632	12137
NEG/DELTA1-03	b11664	50073 ± 2074	323	465	8938
*NEG/DELTA1-03B**	*b11647*	*107265 ± 3929*	*689*	*1013*	*19783*
NEG/DELTA1-03(ii)	b11699	48222 ± 2141	329	468	8882
NEG301	b11637	64298 ± 2516	347	506	9841
NEG302	b11638	53870 ± 2122	292	435	8619
NEG303	b11639	55774 ± 2125	334	500	9932
NEG305	b11640	50871 ± 1930	321	488	9829
NEG306	b11644	41973 ± 2064	368	491	8698
NEG308	b11645	42861 ± 2286	444	572	9622
NEG/MOR/1	b11613	91366 ± 3169	395	602	12113
NEG/MOR/2	b11614	116075 ± 3378	425	716	15354
NEG405	b11646	81816 ± 2926	416	629	12579
NEG502	b11648	59175 ± 2688	346	471	8540
NEG504	b11670	71020 ± 2891	391	558	10623
NEG505	b11650	57178 ± 3513	492	596	8968
*NEG507**	*b11651*	*49964 ± 2250*	*317*	*442*	*8247*
*NEG508**	*b11652*	*61832 ± 2423*	*373*	*545*	*10582*
*NEG510**	*b11653*	*64809 ± 2676*	*441*	*626*	*11840*
NEG511	b11654	45544 ± 2115	334	459	8423
NEG513	b11657	45223 ± 2185	365	495	8924
NEG515	b11658	41048 ± 2021	356	477	8462
*NEG516**	*b11659*	*52798 ± 2362*	*428*	*592*	*10892*
*NEG517**	*b11660*	*35427 ± 1932*	*338*	*440*	*7523*
NEG518	b11661	40303 ± 1988	358	481	8562
NEG519	b11698	39754 ± 1983	341	468	8541

^{26}Al data					
	Accel'r ID	^{26}Al/g Qtz	^{26}Al/^{10}Be	^{26}Al int. error (yr)	^{26}Al ext. error (yr)	^{26}Al LSDn age (yr)
NEG101	*a3088*	*19615068 ± 866975*	*4.5 ± 0.2*	*12339*	*26925*	*245984*
NEG102	*a3084*	*22213145 ± 919295*	*4.5 ± 0.2*	*13603*	*31348*	*284606*
NEG104	*a3089*	*1981622 ± 95153*	*6.0 ± 0.3*	*1401*	*2878*	*28818*
NEG105	a3090	1424417 ± 76301	7.6 ± 0.5	1215	2304	22512
NEG202	a3085	1041223 ±49940	6.0 ± 0.3	756	1551	15624

Samples from transects NEG 2, 3 and 4, the delta DELTA1, and the moraines MOR01 and MOR02 were grouped into one transect for this analysis based on their geomorphic context in relation to ice surface lowering (Lane et al., 2023). Samples were excluded from final analyses of retreat and thinning history if they were older than 30 ka or identified as a likely stratigraphic outlier (Table 2).

The paper assesses thinning and retreat patterns based on a sequential analysis of each vertical transect, before assessing thinning rates using linear and multiple regression techniques. Both spline and piecewise analyses of the dataset were considered to calculate thinning rates (Tables 3 and 4). Lateral retreat rates are also estimated from thinning rates using the approach of Konrad et al. (2018), based on contemporary observations from ice streams in Antarctica.

2.4. Longer term landscape evolution

To consider the effect of complex erosion and burial processes on the apparent exposure ages of high elevation terrain above the limit of warm-based ice (e.g. Roberts et al., 2013; Briner et al., 2014; Beel et al., 2016; Skov et al., 2020) we apply the NUNAIT model (Rodés, 2021). The concentration of cosmogenic isotopes accumulated in samples depends not only on the duration of the surface exposure since the last

Table 3
Vertical thinning rates at each vertical transect calculated using linear regression analysis and retreat rates assuming grounding line retreat of 110 m equates to 1 m of ice thinning (Konrad et al., 2018). The data is split into two periods; 25–10 ka to assess early thinning and post 10ka to assess retreat from the pinning point at Bloch Nunakker.

Based on samples dated to approximately 25–10 ka (early thinning before retreat from Bloch Nunatakker)		
Thickness differences		
Transect	Highest elevation (m)	Lowest elevation (m)	Difference (m)
NEG1	713	320	393
NEG2-3	764	231	533
Estimated thinning rates		
Transect	Lower 68% (ma^{-1})	Upper 68% (ma^{-1})
NEG1	0.0119	0.0445
NEG2-3	0.0446	0.2128
Estimated grounding-line retreat		
Transect	Lower (km)	Upper (km)
NEG1	40.9	45.6
NEG2-3	55.4	61.8
Estimated grounding-line retreat rates		
Transect	Lower 68% (ma^{-1})	Upper 68% (ma^{-1})
NEG1	**1.2**	**5.2**
NEG2-3	4.6	**24.7**

Based on accelerated thinning/retreat from Bloch Nunatakker (post 10ka)		
Thickness differences		
Transect	Highest elevation (m)	Lowest elevation (m)	Difference (m)
NEG1	400	62	338
NEG2-3	423	89	334
NEG5	529	139	390
Thinning rates		
Transect	Lower 68% (ma^{-1})	Upper 68% (ma^{-1})
NEG1	0.1358	0.2941
NEG2-3	0.2383	2.1425
NEG5	0.8044	5.2893
Estimated grounding-line retreat		
Transect	Lower (km)	Upper (km)
NEG1	35.2	39.2
NEG2-3	**34.7**	38.7
NEG5	40.6	**45.2**
Estimated grounding-line retreat rates		
Transect	Lower 68% (ma^{-1})	Upper 68% (ma^{-1})
NEG1	**14.1**	34.1
NEG2-3	24.8	248.5
NEG5	**83.7**	**613.6**

deglaciation, but also on the complete history of the surface, including, exposure during previous interglacials, subaerial and subglacial erosion rates, muon production under ice and rock, and uplift. NUNAIT explores the parameter space for these variables and solves for the set of values consistent with apparent exposure ages. It does this by assuming that former ice elevations can be scaled to climate variations recorded by the global δ^{18}O curve (Rodés, 2021). This carries the simple inference that lower surfaces were beneath thicker ice during glacial periods and, hence, they were glaciated for longer periods. The NUNAIT calculator provides a range of possible values for ice-thinning as well as glacial and interglacial erosion rates that fit our dataset of ^{10}Be and ^{26}Al apparent exposure ages. In the model we use the TYPE 0 default setting assuming the cosmogenic ages reflect the deglaciation trend.

The NUNAIT calculator requires the elevation of the current surface of the ice sheet as an input. We applied an elevational correction of 35, -81, and −163 m asl for the NEG1, NEG2/3, and NEG5 transects respectively. The first elevation is the current ice surface elevation at the base of the NEG1 transect. The other two values correspond to the gradient of a modelled ice surface with a gradient of 3–5° that also fits the vertical offset in the apparent exposure ages from each vertical transect. These data are summarized in the input file NEG.csv (https://github.com/angelrodes/NUNAIT; supplementray information). To accommodate any vertical inaccuracy, the NUNAIT model includes a ±35 m vertical range. An initial screening using the NUNAIT calculator shows that tectonic uplift rates up to 10 m/Ma have a negligible effect.

This infers the NUNAIT model is not sensitive to uplift rates between 0 and 10 m/Ma. Therefore, tectonic uplift is discounted in the models presented.

2.5. Post LGM thinning and retreat rates

Thinning rates for each vertical transect are estimated using linear regression analysis (Jones et al., 2019). The relationship established between thinning and grounding line retreat is then calculated from modern observations based on the work of Konrad et al. (2018) (Table 3).

3. Results

The geomorphic context, distribution and details relating to TCN samples are provided in Figs. 2–6 and Tables 1 and 2 In addition, Lane et al. (2023) provide a geomorphic assessment of the landscape. Fig. 5a excludes ^{10}Be ages over 30 ka. Fig. 5b includes all ^{10}Be exposure ages under 30 ka and highlights possible stratigraphic outliers in grey (see methods). Fig. 6 includes all ^{10}Be and ^{26}Al data. Fig. 7 includes all ^{10}Be exposure ages under 30 ka and with stratigraphic outliers removed.

3.1. Outer fjord (NEG 1)

Vertical transect NEG1 covered an altitudinal range from 1081 to 62 m asl and included both bedrock and erratic samples (Fig. 4a and b; Table 1). Fourteen samples were processed for ^{10}Be and four for ^{26}Al. Above ~900 m asl the terrain is composed of autochthonous quartzite blockfield with occasional in situ outcrops of bedrock which exhibited distinctive weathering pits (Lane et al., 2023). NEG101 and NEG102 were quartzite bedrock samples taken at 1081 and 1077 m asl and provided ^{10}Be ages of 420 ± 20.1 and 486 ± 24.0 ka respectively (Table 2). These ages do not closely match the corresponding ^{26}Al ages of 246 ± 26.9 ka and 285 ± 31.3 ka indicating a complex exposure/burial history (Table 2). Between ~900 m and 600 m asl the terrain transitions to allochthonous blockfield with an increasing abundance of glacial erratics of multiple lithologies (e.g. sandstone, limestone, granite; gneiss; Fig. 4c) (Lane et al., 2023). Bedrock outcrops are rare and often lack signs of glacial abrasion. Samples NEG104, 105 and 106 (bedrock and erratic samples; 806–619 m asl) provided exposure ages of 36.8 ± 1.8, 22.9 ± 1.1 and 18.9 ± 0.9 ka respectively (Table 2). Corresponding ^{26}Al ages for NEG104 and NEG105 were 28.8 ± 2.9 and 22.5 ± 2.3ka suggesting simple exposure histories.

From 600 m asl down to sea-level the terrain becomes heavily glacially abraded and streamlined with areas of areal scour and well developed roches moutonnées at lower elevations along the fjord wall (Lane et al., 2023). (Fig. 4d.). The steep terrain lacks thick glacial sediment, but erratics are ubiquitous and linear swathes of glacial debris mark weathered moraines. Periglacial activity is common with solifluction lobes and stripes. NEG109 at 532 m asl has a ^{10}Be age of 27.0 ± 1.3 ka. NEG114-117 range in age from 10.4 to 9.2 ka between 400 and 320 m asl. Below 300 m NEG119 and NEG121 provide ages of 9.2 ± 0.5 and 7.8 ± 0.4 ka respectively on heavily streamlined bedrock terrain. NEG122 and NEG123 provide exposure ages of 8.2 ± 0.4 and 7.3 ± 0.4 ka just above the local marine limit on Hovgaard Ø. Paired samples often provide slightly different ages, but bedrock samples do not appear systematically older in relation to possible isotope inheritance (Table 2). Directly south of Hovgaard Ø, three exposure ages above the marine limit (72 and 76 m asl) on the pinning point known as Bloch Nunatakker constrain ice free conditions to 9.1 ± 0.9, 8.6 ± 0.9 and 9.2 ± 0.9 ka respectively (G1614, 1616, 1617; Larsen et al., 2018).

3.2. Mid fjord (NEG2 – 3)

Vertical transects NEG 2 and 3 cover an altitudinal range of 764 to 89 m asl (Figs. 3–5). The samples were a mix of bedrock and erratics

Table 4
Summary retreat and thinning rates from this study compared to retreat and thinning rates derived from other palaeoglacioloical studies in Greenland (italicised) and contemporary thinning and retreat rates observed from the NEGIS (Khan et al., 2022) (**bold**). Note site codes for Fig. 9 are included.

Drainage basin	Retreat rate Min (ma⁻¹)	Retreat rate Max (ma⁻¹)	Thinning rate Min (ma⁻¹)	Thinning rate Max (ma⁻¹)	Fig. 9 site code	Source
79N Piecewise (Pre 10 ka)	4	5	0.035	0.041	1	*This study*
79N Piecewise (Post 10 ka)	19	29	0.174	0.263	2	*This study*
79N Linear (Post 10 ka) NEG1	15	32	0.136	0.294	3	*This study*
79N Linear (Post 10 ka) NEG2/3	26	236	0.238	2.143	4	*This study*
79N Linear (Post 10 ka) NEG5	88	582	0.804	5.289	5	*This study*
UISS (Deglacial)	*94*	*121*	*0.85*	*1.10*	6	*Roberts et al. 2013; Lane et al. 2014*
UISS (Early Holocene)	*10*	*70*	*0.09*	*0.64*	7	*Roberts et al. 2013; Lane et al. 2014*
JI (Deglacial)	*104*	*137*	*0.95*	*1.25*	8	*Long and Roberts, 2003; Lloyd et al., 2006; Ó Cofaigh et al., 2013; Young et al. 2011)*
JI (Early Holocene)	*17*	*104*	*0.15*	*0.95*	9	*As above*
NEGIS ZI front	**88**	**385**	**0.8**	**3.5**	10	***Khan et al. (2022)***
NEGIS (2011–2021) 79N grounding line	**55**	**165**	**1.5**	**1.5**	11	***Khan et al. (2022)***
NEGIS (2011–2021) main trunk up to 200 km inland	**22**	**33**	**0.3**	**0.3**	12	***Khan et al. (2022)***
NEGIS (2050–2100) upstream (250 km inland)	**220**	**440**	**2.0**	**4 .0**	13	***Khan et al. (2022)***

Additional site codes (see *Fig. 10*).
14 – Mount Rea, Antarctica (*Small* et al. *2019*) - PALAEO.
15 – Gondola Mid-Lower (*Small* et al. *2019*) – PALAEO.
16 – Pine Island Glacier (*Konrad* et al. *2018*) - CONTEMP[Y].
17 – Totten Glacier (*Konrad* et al. *2018*) - CONTEMP[Y].
18 – Thwaites Glacier (*Konrad* et al. *2018*) - CONTEMP[Y].
19 - Haynes Pope Smith and Kohler Glaciers (*Konrad* et al. *2018*) – CONTEMP[Y].

(Tables 1 and 2). Twenty samples were processed for ¹⁰Be analysis. Unlike the very steep terrain of NEG1, the terrain adjacent to NEG2 and NEG3 was characterised by hilly, undulating topography separated by low to medium gradient slopes. Several samples were collected from NEG4 slightly further west but only one was selected for ¹⁰Be analysis.

High elevation terrain between 800 and 600 m asl is dominated by gently-sloping allochthonous blockfield terrain but bedrock outcrops and glacial erratics are common. The bedrock outcrops are often frost shattered and weathered but exhibit signs of glacial abrasion particularly where quartzite is present. Samples NEG202-204 and NEG206 cover an elevation range of 764–671 m asl and provide TCN ages of 20.1 ± 0.9, 14.7 ± 0.7, 10.9 ± 0.5 and 43.8 ± 2.0ka respectively (Table 2). NEG208, 209 and 211 are located between 596 and 490 m asl and provide exposure ages of 44.4 ± 2.0, 11.6 ± 0.6 and 15.4 ± 0.8 ka. Thus, there is no clear pattern of ice thinning between 764 and 490 m asl. Below 500 m, glacial erratics become more ubiquitous and allochthonous blockfield transitions to glacial drift interspersed with bedrock outcrops (Fig. 4 d-f). NEG3 samples run from 465 m asl to 89 m asl with exposure ages ranging between 9.9 and 8.6 ka (Tables 1 and 2). The ages all broadly overlap within error limits.

To supplement the exposure ages derived from NEG2 and NEG3 several moraines and ice marginal deltas were mapped and dated in the mid fjord area (Lane et al., 2023, Fig. 4e–g). The highest elevation ice stream marginal moraines occur at ∼600–650 m asl, close to the NEG3 transect. Two samples (MOR01 and MOR02) from erratics on the crest of a moraine provided exposure ages of 15.3 ± 0.7 and 12.2 ± 0.6 ka, respectively (Table 2). A lower moraine in the sequence (located between 480 and 400 m asl) is constrained by a single exposure age (NEG405) of 12.6 ± 0.6 ka (Table 2).

Closely associated with the moraines are glaciolacustrine deltas formed through damming of ice marginal drainage during ice stream thinning (Lane et al., 2023). These range in elevation between 520 and 50 m asl and are common along the mid fjord above the local marine limit (Fig. 4g). In many cases the topset surfaces are well preserved and composed of well sorted, cobble sized material. A set of delta surfaces

between 315 and 284 m asl provided four exposure ages. The highest surface at 315 m asl was dated to 12.1 ± 0.6 ka (DELTA1-01). The middle surface at 291 m asl provided two ages of 8.9 ± 0.5 and 8.8 ± 0.5 ka (DELTA1-03 and DELTA1-03ii), while the lowest surface at 284 m asl proved to be much older at 19.8 ± 1.0 ka, suggesting inheritance (DELTA1-03 B; Table 2).

3.3. Inner fjord (NEG 5)

Vertical transect NEG5 overlooks the contemporary grounding line of 79N Glacier and ice shelf. In this region, adjacent to Blåsø epishelf lake, the terrain is mainly hilly with periglacially reworked glacial drift forming solifluction lobes and stripes. TCN samples ranged in elevation between 529 and 115 m asl and were predominantly erratics (Fig. 3).

Samples NEG502 to NEG519 yield a relatively narrow range of ages between 11.8 and 7.5 ka, though display little systematic pattern of ice thinning and decreasing exposure age (Figs. 3 and 5). However, there are two clear clusters of ages in this transect: one with ages between 11.8 and 10.6 ka (Table 2; NEG504, 508, 510, 516); another with a cluster of eight samples that date to between 9.0 and 8.2 ka (NEG502, 505, 507, 511, 513, 515, 518, 519; Table 2). NEG517 at 171 m asl is the youngest with an exposure age of 7.5 ± 0.4 ka (Table 2). Three pre-existing TCN samples from erratics just to the northwest of Blåsø (190-108 m asl) provide exposure ages of 12.0 ± 1.5, 10.2 ± 0.5 and 7.8 ± 2.7ka respectively (GL1522-24; Larsen et al., 2018).

Overall, NEG 1 and NEG 2/3/4 show slower thinning between 20 and 10 ka above ∼450 m asl. All three transects including NEG5 show an increase in thinning rates post-10 ka and below ∼450 m asl.

3.4. Patterns and rates of change

In order to fit the distribution of ¹⁰Be and ²⁶Al exposure ages reported here, the NUNAIT calculator suggests a total magnitude of ice-thinning during deglaciation of 1011 and 938 m, with most likely subaerial erosion rates between 1.2 and 1.9 m/Ma and glacial erosion rates

Fig. 4. Terrain bordering Nioghalvfjerdsfjorden and selected geomorphic landforms and associated surface exposure age samples. a) NEG 1: An overview of the eastern end of Nioghalvfjerdsfjorden with the Bloch Nunatakker pinning point in background at the edge of the ice shelf. Autochthonous quartzite blockfield at ~1000 m asl in the foreground. b) NEG 1: Autochthonous quartzite blockfield on the summit of Hovgarrd Ø at ~1000 m asl. c) NEG 2: Erratic on allochthonous blockfield at ~800 - 700 m asl near Midgårdsormen. d) NEG 1: Heavily glacially abraded gneissic bedrock with perched erratics at ~100 m asl. The local marine limit occurs just below this on Hovgaard Ø at 65–70 m asl. e) A lateral moraine marking the edge of the ice stream at ~400 m asl to the east of Blåsø epishelf lake. f) Lateral moraine passes into 'hummocky' moraine composed of conical mounds and kettle holes at ~400 m asl in the vicinity of Iskadalen. g) A perched delta marking ice dammed lake formation during ice stream thinning at ~300 m asl to the east of Iskadalen.

5a

5b
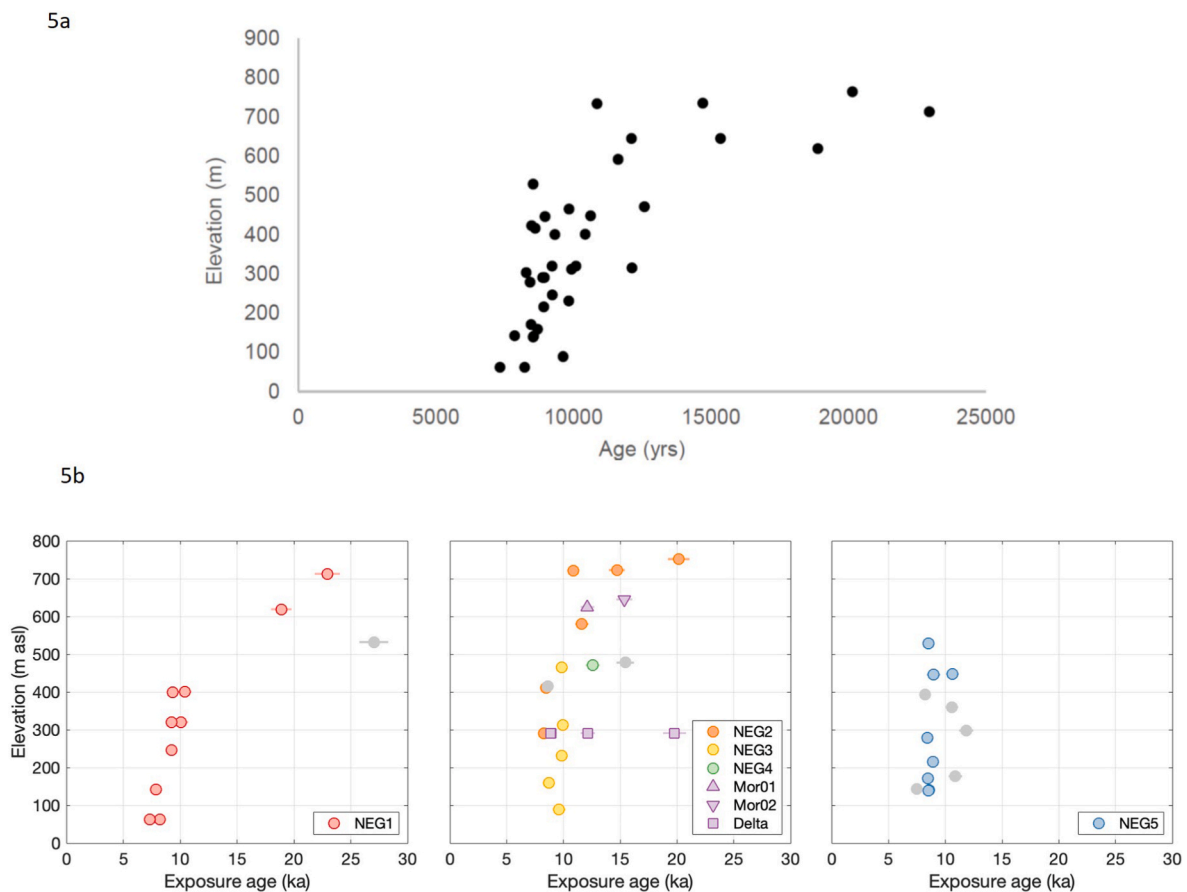
Fig. 5. a) [10]Be surface exposure ages (LSDn) from the northern edge of Nioghalvfjerdsfjorden. Exposure ages are plotted against elevation. Error bars are plotted at 1-sigma. Samples with [10]Be ages over 30 ka are removed (see methods section). b) [10]Be surface exposure ages from each vertical transect plotted independently (age against elevation). Overall, NEG 1 and NEG 2/3/4 show slower thinning between 20 and 10 ka above ~450 m asl. All three transects including NEG5 show an increase in thinning rates post 10 ka and below ~450 m asl. 'Likely outliers' as defined using a stratigraphic approach are plotted in grey (see methods).

between 7.4 and 88 mm a^{-1} (Fig. 6a). These results broadly agree with interglacial and glacial and erosion rates obtained by Skov et al. (2020) of <3 m/Ma and >20 m/Ma respectively. Guided by the vertical distribution of apparent exposure ages and global δ^{18}O curve, the best-fit NUNAIT models show a stepped profile with three broad thinning stages below 1000 m asl (Fig. 6b; 1000–800 m, 800 to 600 m; 600 to 0 m).

The onset of ice stream thinning is best constrained by NEG105, NEG202 and NEG106 (22.9 ka, 20.1 ka and 18.9 ka respectively) between 764 and 619 m asl in the outer to mid fjord (Table 2; Figs, 5 b). Based on the mid fjord transect, thinning continues from 735 m asl and from the high elevation moraine at 645 m asl and is constrained to 15.3–14.7 ka. Between 645 m asl and 465 m asl further thinning is constrained to 12.1 ka and 9.8 ka (Tables 1 and 2). Below 465 m asl the whole length of the fjord deglaciates from ~10.0 to 7.5 ka with many exposure ages overlapping (Fig. 5b).

Post LGM, ice stream thinning rates are estimated using piece-wise regression and grounding line retreat projections based on Konrad et al. (2018) (Fig. 7). This regression used the relative elevation of each sample above the modern ice surface and the mean age ±1 st.dev. Within a Monte Carlo framework (10,000 iterations). By statistically partitioning into a two-phase thinning history, the analysis identified a break point centred at 10.4 ka (median) (9.9–10.8 ka; 68% confidence). Estimated thinning rates are 0.03 ma^{-1} for the first phase when ice lowered from ~800 to 500 m asl between 22.9 ka and 10.4 ka. In the second phase, post-10.4 ka, average thinning rates increase by an order of magnitude to 0.20 ma^{-1}. We hypothesise that this coincides with a rapid, fjord-wide deglacial event, with terrain below ~500 m asl

becoming ice free as the ice unpinned from Bloch Nunatakker and receded from the outer coast.

To test the assertion above of a 'rapid, fjord-wide deglacial event', this study further assesses the timing and rates of thinning for individual vertical transects relative to the reported retreat from Bloch Nunatakker (at 8.9 ± 0.3 ka, weighted mean; Larsen et al., 2018). Linear regression analysis was executed in two phases for transects NEG1, 2 and 3 combined, and 5. Firstly, for sample ages older or consistent with the date of Bloch Nunatakker retreat (excluding NEG5 as there were not enough ages), and secondly, for ages younger or consistent with the retreat date (Fig. 8).

Consistent with the piecewise analysis, initial thinning prior to retreat at Bloch Nunatakker was relatively slow at NEG1 (~0.04 ma^{-1}) and NEG2/3 (0.2 ma^{-1}), corresponding to predicted grounding line retreat rates of 5.2 m a^{-1} and 24.7 m a^{-1} respectively (Table 3). This initial phase of retreat must have occurred through the inner to mid continental shelf as offshore chronological constraints show the grounding line on the mid to inner continental shelf in that time window (Syring et al., 2020; Davies et al., 2022; Lloyd et al., 2023). Once the ice stream ungrounded from Bloch Nunatakker, thinning rates both increased and accelerated up fjord, approaching 2.1 to 5.2 ma^{-1} through the mid to inner fjord (Fig. 8a). These are an order of magnitude higher than the post-10.4 ka piecewise regression estimates that utilised the full dataset (~0.20 ma^{-1}) (Table 3), highlighting much faster thinning at specific points along the ice stream occurred compared to an overall average. Retreat rate estimates through Nioghalvfjerdsfjorden also demonstrate increasingly rapid westwards grounding line retreat in the order of 248–613 ma^{-1}. As deglaciation was finished at NEG2/3 and
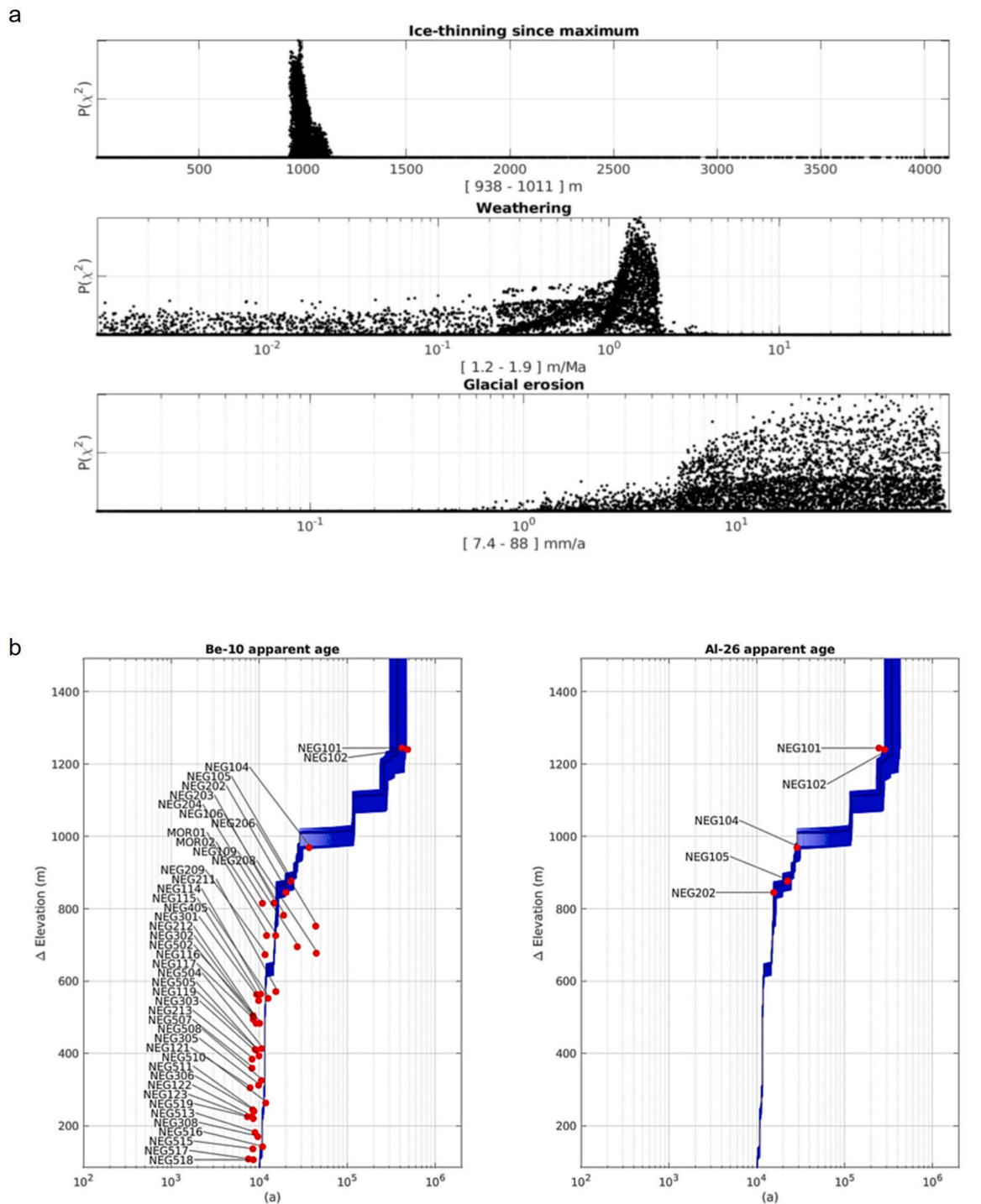
a

b

Fig. 6. a) Probability distribution of the NUNAIT models fitting the data for each parameter: ice thinning since maximum glacial extent, subaerial erosion rate (weathering) and subglacial erosion rate. Vertical axis represents the relative likelihood of each model. Note that all the models consider an uplift rate of 0. b) Elevation profiles of the apparent exposure ages for the best fitting model (black line) and all NUNAIT models fitting the data within one-sigma confidence level (blue lines). The actual apparent exposure ages of the samples are depicted by red dots. Vertical axis shows elevation with respect to the current ice surface assuming 35 m of uncertainty. Left: ^{10}Be. Right: ^{26}Al.

NEG5 by the time it ended at NEG1, all transects support a 'rapid deglacial event' coincident with retreat from Bloch Nunatakker (Fig. 8b).

4. Discussion

4.1. Cold v warm-based ice in the landscape

In the outer fjord the lack of correspondence between several ^{10}Be and ^{26}Al ages above 1000 m asl points to a complex exposure/burial history across these high elevation surfaces (Table 2). Together with in
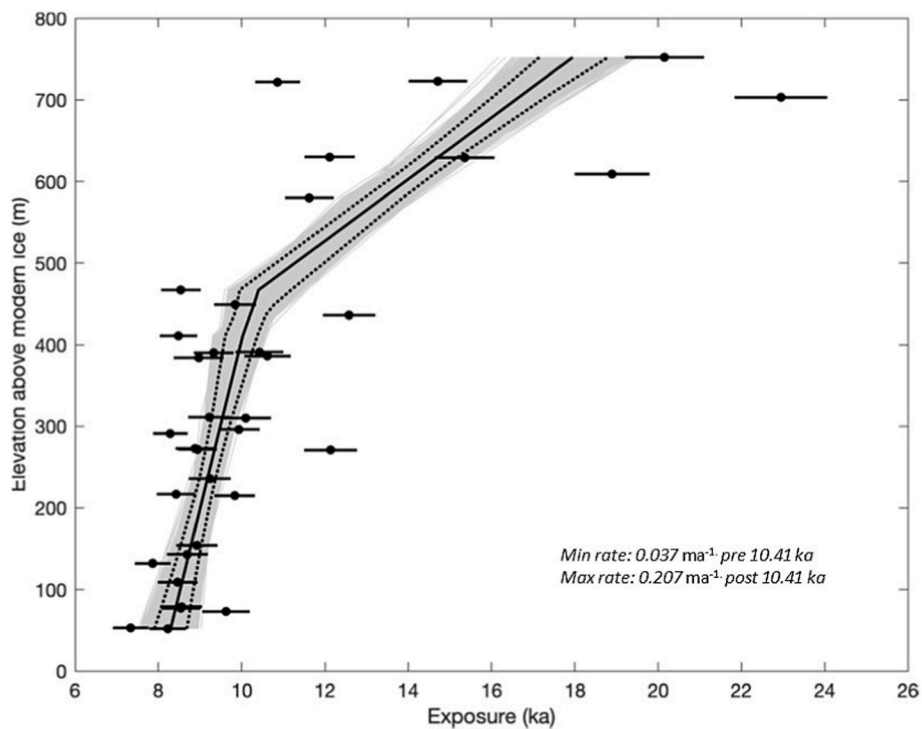
Fig. 7. A piecewise analysis of the TCN data set which identifies a distinct two stage thinning history for the ice stream. Prior to 10.4 ka the model calculates slow thinning at 0.037 ma⁻¹, but, post this inflexion point thinning rates increase five-fold to 0.207 ma⁻¹. Error bars are plotted at 1 sigma.
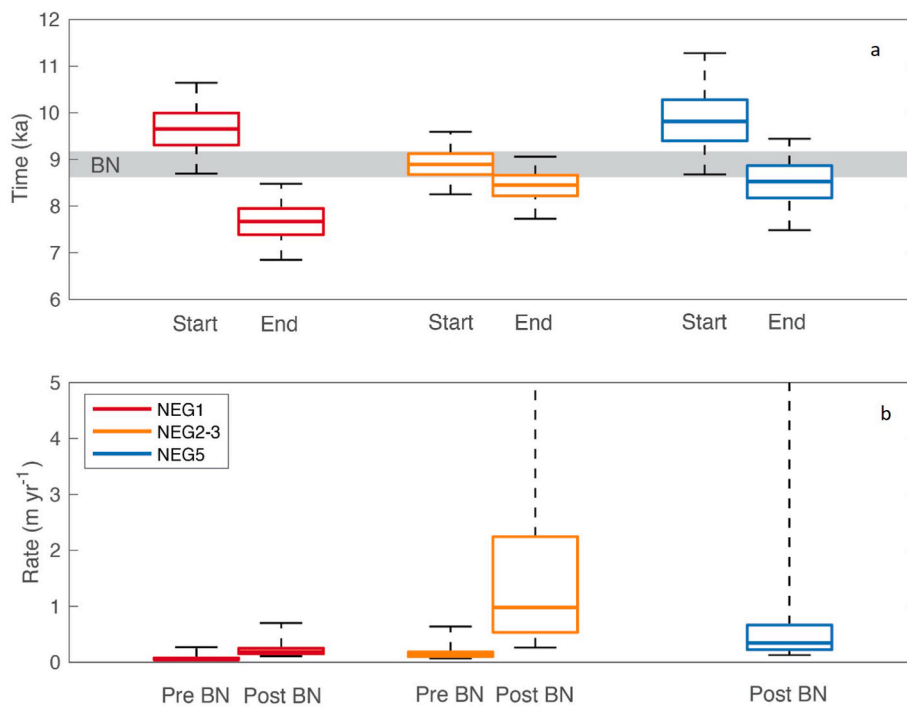
Fig. 8. a) TCN ages postdating 10.0 ka from outer (NEG1), mid (NEG 2/3) and inner fjord (NEG 5) compared to the onset of grounding line retreat west from Bloch Nunatakker (grey bar). All of the outer, mid, and inner fjord transects record thinning consistent with the timing of retreat from Bloch Nunataker at ~8.6 ka. For each box-whisker, the horizontal bar represents the median, and the box and whiskers represent the 68% and 95% ranges respectively b) Linear rate analysis showing thinning rates accelerated up fjord once ice ungrounded from Bloch Nunatakker. This linear rate projection is an order of magnitude higher than the piecewise regression estimates post 10.4ka (~0.20 m a⁻¹).

situ weathering pits, the lack of glacially moulded surfaces and the presence of autochthonous blockfield this indicates the presence of cold-based ice, or long-term exposure to periglacial conditions, or a mixture of both, with minimal glacial erosion experienced over extended time periods (Rea et al., 1996; Beel et al., 2016; Ballantyne, 2018; Strunk et al., 2017). In Dove Bugt, to the south of the study area, paired

^{10}Be/^{26}Al nuclide samples from bedrock and erratics between 900 and 500 m asl. have been used to infer slow rates of plateau erosion from 0.6 to 1.0 Ma (Skov et al., 2020). In contrast, from 0.6 Ma onwards, Skov et al. (2020) imply a switch to selective linear erosion which drove fjord over-deepening and led to the retardation/cessation of ice sheet erosion on high-level surfaces. This scenario also applies to the high elevation areas peripheral to Nioghalvfjerdsfjorden where autochthonous block-field is present.

Skov et al. (2020) used the model of Knudsen et al. (2015), which assumes that the ice-sheet evolution couples to the δ^{18}O record, as does the NUNAIT model employed herein (Rodés, 2021). However, while the NUNAIT model is usually fitted to a vertical profile of data, the model employed in Knudsen et al. (2015) can be fitted to data from a single site. This makes NUNAIT model more sensitive to the vertical distribution of apparent exposure ages, and the model of Knudsen et al. (2015) more sensitive to diverging ^{26}Al/^{10}Be ratios. Moreover, the Knudsen et al. (2015) model is designed to resolve the shortest possible histories (i.e. it is designed to calculate minimum landscape ages), whereas the NUNAIT considers the longest possible history of cosmogenic nuclide accumulation. Hence, NUNAIT simulates the muon-produced cosmogenic nuclides at greater depths and under the ice. Despite these differences, both models yield similar exposure-burial histories for thick ice sheets (hundreds of meters) and erosion rates greater than 1 m/Ma.

As both glacial and interglacial erosion rates are modelled by NUNAIT, it is possible to reconstruct the evolution of each surface back in time and, therefore, to date the onset of the glaciation in the area. In this case, the modelled evolution of these surfaces suggests glacial erosion started either during Marine Isotope Stage (MIS) 16 (676–621 ka) or MIS 12 (478–424 ka) (Fig. 9). This correlates with the two largest glacial periods in Quaternary history when ice thickness and extent in NE Greenland may have been sufficient to initiate high elevation warm-based glacial erosion, selective linear erosion and trough over-deepening (Sugden, 1974). Before this time, these surfaces were likely continuously above the ice sheet surface and eroding slowly under subaerial/periglacial conditions. The MIS 16 and MIS 12 predictions concur with minimum accumulation ages of 0.6–1 m/Ma proposed by Skov et al. (2020). These represent a minimum age for the summit plateaux;, but post-0.6 Ma such surfaces have been subjected to complex burial and exposure histories with cold-based ice caps periodically developing over blockfield covered summits.

Between 900 and 600 m asl allochthonous blockfield and poorly-developed glacially-abraded bedrock surfaces point to a transition landscape experiencing a change from cold to warm-based ice (Lane et al., 2023). In this elevational range, erratics were potentially transported and deposited by cold-based ice, though it is also conceivable that such allochthonous blockfields developed from Late Pliocene to Mid Pleistocene till cover. The former hypothesis is supported by Skov et al. (2020) who demonstrate that erratics from summit areas on Store Koldeway and Pusterdal were emplaced by cold-based ice across high elevation plateau surfaces during the last glacial cycle (deglacial dates of 12.3–12.4 ka; Skov et al., 2020). Several erratics sampled along the margins of 79N fjord between 800 and 600 m asl adhere to such a subglacial thermal model and, in addition, this partially explains isotope inheritance in several bedrock samples (Tables 1 and 2; e.g. NEG206, NEG208). Below 600 m both the geomorphic signal and simple ^{10}Be exposure histories support a transition to erosive, warm-based ice (Lane et al., 2023).

4.2. Ice stream thinning during initial deglaciation and at the LGM-holocene transition

The exposure age of sample NEG 105 (713 m asl) with its paired ^{10}Be/^{26}Al ages of 22.9 and 22.5 ka provides the best constraint on initial thinning in the outer fjord (Table 2). This paired isotope age marks the onset of LGM deglaciation for NE Greenland. The additional ages of 20.9 and 18.9 ka from NEG202 and NEG106 respectively further constrain
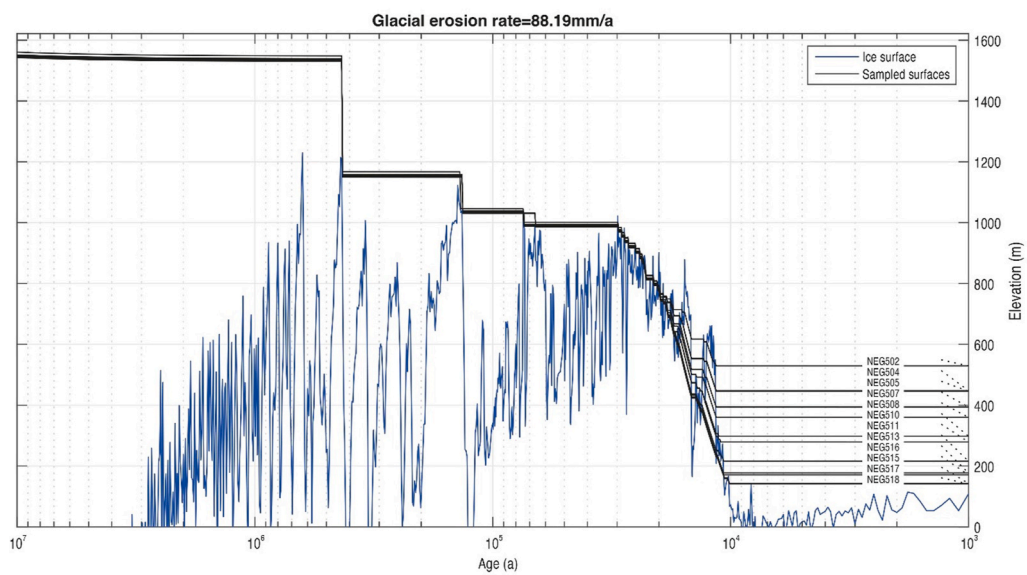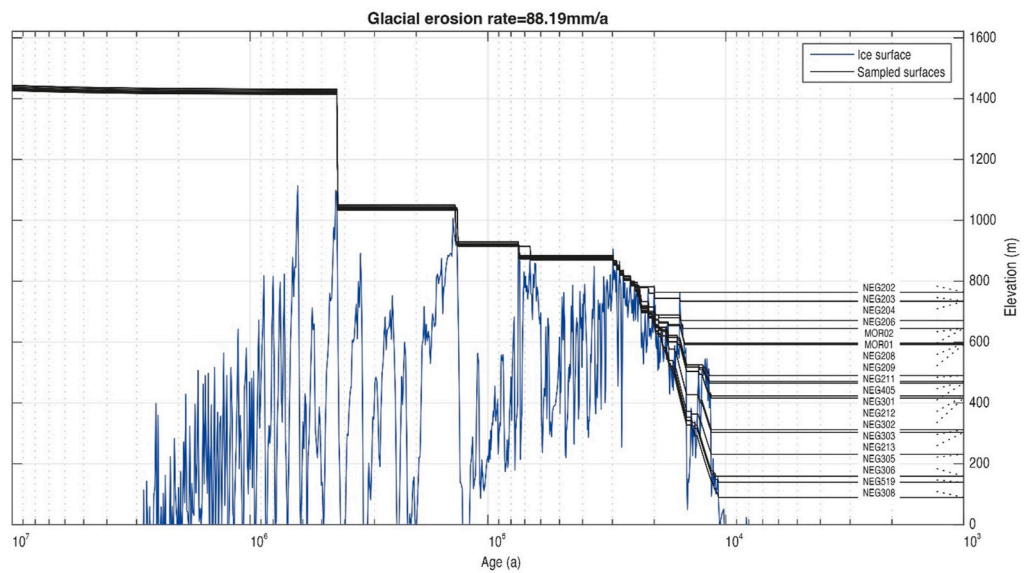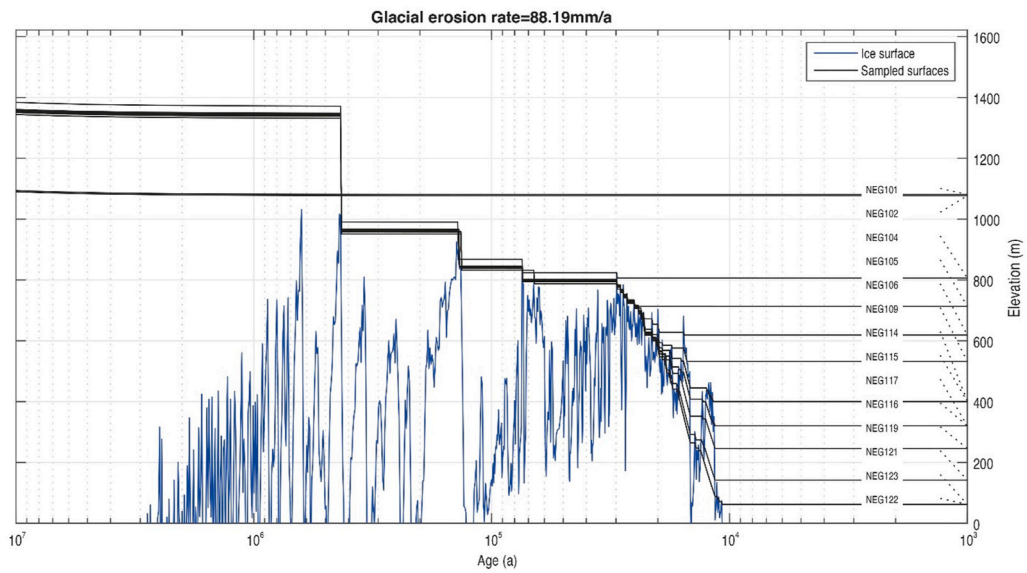
the beginning of deglaciation at high elevation. In the mid fjord, ongoing thinning from 735 m asl and from the high elevation moraine at 645 m asl is constrained to 15.3–14.7 ka. Together, these exposure ages place the ice surface above 600 m asl between ~23 and 15 ka and imply ice reached the continental shelf edge at the LGM, supporting several previous assertions (Evans et al., 2009; Arndt et al., 2015, 2017), though Rasmussen et al. (2022) have recently questioned a shelf-edge LGM glacial model.

Based on our TCN evidence, ice surface lowering may have preceded grounding line retreat from the continental shelf edge by two to three thousand years. However, when ice did start to withdraw from the continental shelf edge, accelerated thinning would have triggered further concomitant draw-down of inland ice. Lane et al. (2023) identified a clear geomorphic signal of ongoing ice stream surface lowering below ~650 m asl. This is manifested in nested lateral moraines and delta staircases which infer quasi-ice marginal (in)stability during initial deglaciation, though the exact timing of this thinning is challenging to interpret due to age reversals (Table 2). This quasi-(in)stability may have been partially influenced by grounding line behaviour across the continental shelf resulting from changes in bathymetry, thinning rates, and ice shelf presence/absence. Arndt et al. (2017) also report grounding zone wedges in Norske Trough and De Geer moraines occur in Westwind Trough (Winkelmann et al., 2010); all indicative of grounding line instability.

Adopting the approach taken by Konrad et al. (2018) suggests retreat rates of 1.2 ma^{-1} and 24.7 ma^{-1} when the grounding line was on the mid to inner continental shelf between 23 and 10 ka. However, post ~10 ka thinning and grounding line retreat accelerated as the fjord began to deglaciate (Tables 3 and 4). At NEG1 grounding line retreat rates approached 14.1–34.1 ma^{-1} as ice withdrew from the inner continental shelf, but these changed dramatically upstream where retreat rates peaked at 613 ma^{-1} at NEG5 in the inner fjord (based on 5.2 ma^{-1} thinning). Both Bennike and Weidick (2001) and Smith et al. (2023) point to the deglaciation of Blåsø and the formation of the marine limit on its western shores by 8.5 ka. Hence, the deglacial record shows complete grounding line retreat (and ice shelf disappearance) to the inner fjord by 8.5 ka. Given Nioghalvfjerdsfjorden is over 900 m deep, with a reverse bedrock slope between Bloch Nunatakker and Blåsø, this dramatic acceleration in grounding line retreat rate suggests marine ice sheet instability played a role in governing ice stream dynamics at this time.

These estimates of thinning and retreat rates during the LGM to Holocene transition are similar to other palaeo GrIS ice stream systems such as Uummannaq Ice Stream (UISS) and Jakobshavn Isbrae (JI) (Fig. 10). During deglaciation from the outer to inner continental shelf the UISS grounding line retreat rates varied from 121 to 94 ma^{-1} between ~14.9 and 11.5 ka as ice withdrew through the deep Uummannaq Trough. From 11.5 to 5.0 ka these rates slowed to 70 - 10 ma^{-1} due to fjord narrowing (Roberts et al., 2013; Lane et al., 2014). JI similarly experienced grounding line retreat rates in the order of 137–104 ma^{-1} as ice withdrew through Disko Bugt between 12.5 and 10.2 ka (Lloyd et al., 2005; Ó Cofaigh et al., 2013). Retreat rates subsequently slowed to 17 ma^{-1} between 10.2 ka to 7.4 ka as ice retreated through the narrow confines of JI (Long and Roberts, 2003; Young et al., 2011, Fig. 10).

Recent observations from NEGIS show accelerating thinning near the grounding line of both 79N Glacier and ZI between 2011 and 2021 (79N: 0.5–1.5 ma^{-1}; ZI: 0.8–3.5 ma^{-1}; Khan et al., 2022). Thinning also extended upstream in this time window with the main trunk of NEGIS (up to 200 km inland) exhibiting surface thinning of 0.2–0.3 ma^{-1}. Khan et al. (2022) also suggest NEGIS thinning will accelerate further to 2.0–4.0 ma^{-1} and extend upstream up to 250 km inland between 2025 and 2100. ZI will also retreat 30 km upstream, with dynamic thinning reaching the interior of the GrIS by 2100. Such changes could fundamentally alter the dynamics of the NEGIS system, resulting in the 79N Glacier changing flow direction to subsequently flow out through the ZI gateway. This may be analogous to the Holocene flow phase switch
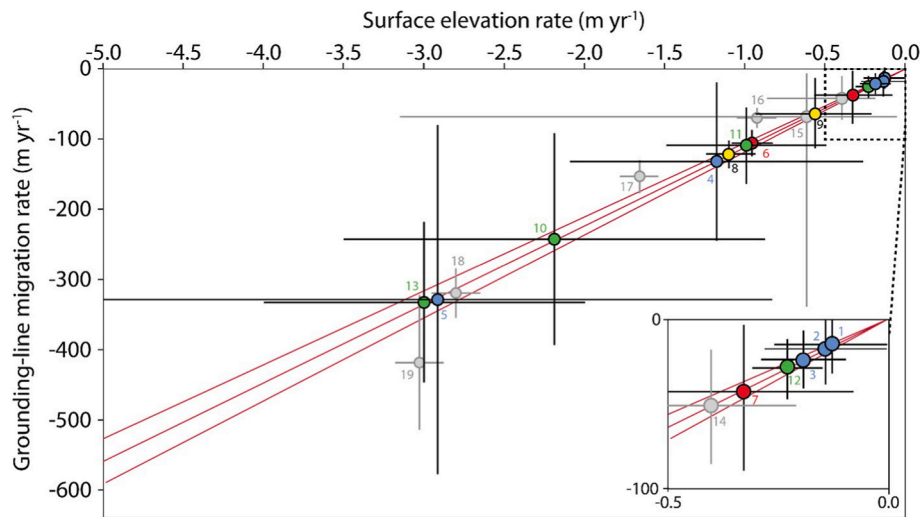
(caption on next page)

Fig. 10. Palaeo and contemporary examples of thinning and grounding line retreat rate for ice stream catchments in Greenland and Antarctica compared to the NEGIS (adapted from Konrad et al., 2018). Recent observations from NEGIS (Green circles) show thinning near the grounding line of both 79NG and Zachariaeæ isstrøm between 2011 and 2021 (79N: 0.5–1.5 m/yr; ZI: 0.8–3.5 m/yr. Thinning also extended upstream in this time window with the main trunk of NEGIS (up to 200 km) exhibiting surface thinning of 0.2–0.3 m/yr. NEGIS thinning rates at the opening of the Holocene (Blue circles) were also commensurate with contemporary thinning rates observed in large Antarctic ice stream drainage basins such as Totten and Thwaites. Site codes are given in Table 4.

recently identified from ice radar data by Franke et al. (2022) and serves to highlight that large scale dynamic changes in ice systems can occur on sub-centennial to millennial scales (cf. Small et al., 2019).

The NEGIS thinning/retreat rates reported here also sit within the range of contemporary and palaeo observations for marine terminating ice streams in Antarctica (Johnson et al., 2014; Jones et al., 2015; Konrad et al., 2018; Small et al., 2019; Stokes et al., 2022) (Fig. 10.). The reasons for both the pattern and rates of thinning and grounding line retreat on the NEGIS are discussed in detail below, however, Konrad et al. (2018) comment on the potential overriding controls of ice-stream surface topography, a sliding bed and bedrock topography in governing grounding line response to thinning; their study noting a 'consistent geometry-driven propensity for retreat' triggered by a coupled relationship between thinning and retreat irrespective of the forcing mechanisms driving ice stream recession. This should be noted with respect to the potential bathymetric controls on the early Holocene retreat history of 79N Glacier through Nioghalvfjerdsfjorden.

4.3. Forcing mechanisms

The initial slow rate of NEGIS thinning at high elevation broadly coincides with onset of LGM deglaciation and climate amelioration across the North Atlantic and Greenland (Fig. 11). The NGRIP record of JJA summer air temperatures shows an upturn during this time (Fig. 11e; Buizert et al., 2018), though surface ablation rates would have remained low at high elevation. Offshore records also show ocean temperatures remained cool with extensive sea-ice cover between ~23 and 15 ka in the Fram Strait region (Devendra et al., 2022, Fig. 11c). This was despite the continuous presence of Atlantic Water (AW) transiting through Fram Strat (Müller et al., 2012; Rasmussen et al., 2022). Devendra et al. (2022) report a slight increase in AW advection on to the shelf between 18.5 and 16.5 ka, but this is offset by a reduction in Arctic Atlantic Water (AAW) indicator species, so sub-surface ocean heat flux remained muted. Thus, while our surface exposure ages point to thinning and the onset of deglaciation between 23 and 15 ka, both

atmospheric and oceanic conditions remained cold and polar during this time with low productivity and extensive sea-ice.

From ~15 to 14 ka there is a marked increase in the JJA air temperature during the onset of Greenland Interstadial 1 (GI-1), accompanied by increased AW flux along the margins of the NE Greenland shelf as indicated by the *Cassidulina neoteresis* record from ~14 ka onwards (Fig. 11d) (Devendra et al., 2022; core GR 02). During this period ice was in full retreat from the outer to mid continental shelf, but chronological constraints on the mid shelf remain poor with only limited deglacial ages between 13.4 ka cal BP to 10.1 ka cal BP (Syring et al., 2020; Pados-Dibattista et al., 2022; Hansen et al., 2022; Davies et al., 2022; Lloyd et al., 2023). Thinning rates in Nioghalvfjerdsfjorden remained relatively low through GI-1 and during Greenland Stadial 1 (GS-1 (Younger Dryas); ~12.8–11.7 ka; Fig. 7). During this period, both increasing insolation and ocean heat flux most likely influenced ice stream surface and submarine (ice shelf and grounding line) melt rates. Arndt et al. (2017) speculated the ice remained on the mid-shelf during GS-1, but our results do not corroborate this.

JJA air temperatures at 79N Glacier remained below 0 °C throughout GS-1 but increased rapidly at 11.7 ka as the stadial terminated. Insolation values continued to rise during GS-1, but surface melt rates will have remained low (Buizert et al., 2018). In contrast, it is evident from several core sites stretching from the Fram Strait eastwards along Norske Trough, that warm AW accompanied grounding line retreat across the continental shelf with rapidly increasing temperatures (2–6 °C) from ~12.0 ka onwards (Werner et al., 2016; Davies et al., 2022, Fig. 11 c, d, f). This would have had a significant impact on submarine melt rates causing grounding line instability and retreat, with a concomitant increase in ice flux, ice drawdown and inland thinning through the coastal fjords. Together with increasing JJA air temperatures of 0–2.5 °C between 11.7 and 11.0 ka, these two forcing mechanisms will have been pivotal in preconditioning the NEGIS for retreat to the coast and collapse through Nioghalvfjerdsfjorden post ~10ka.

Syring et al. (2020) and Lloyd et al. (2023) report deglaciation through the inner Norske Trough to the mouth of Nioghalvfjerdsfjorden
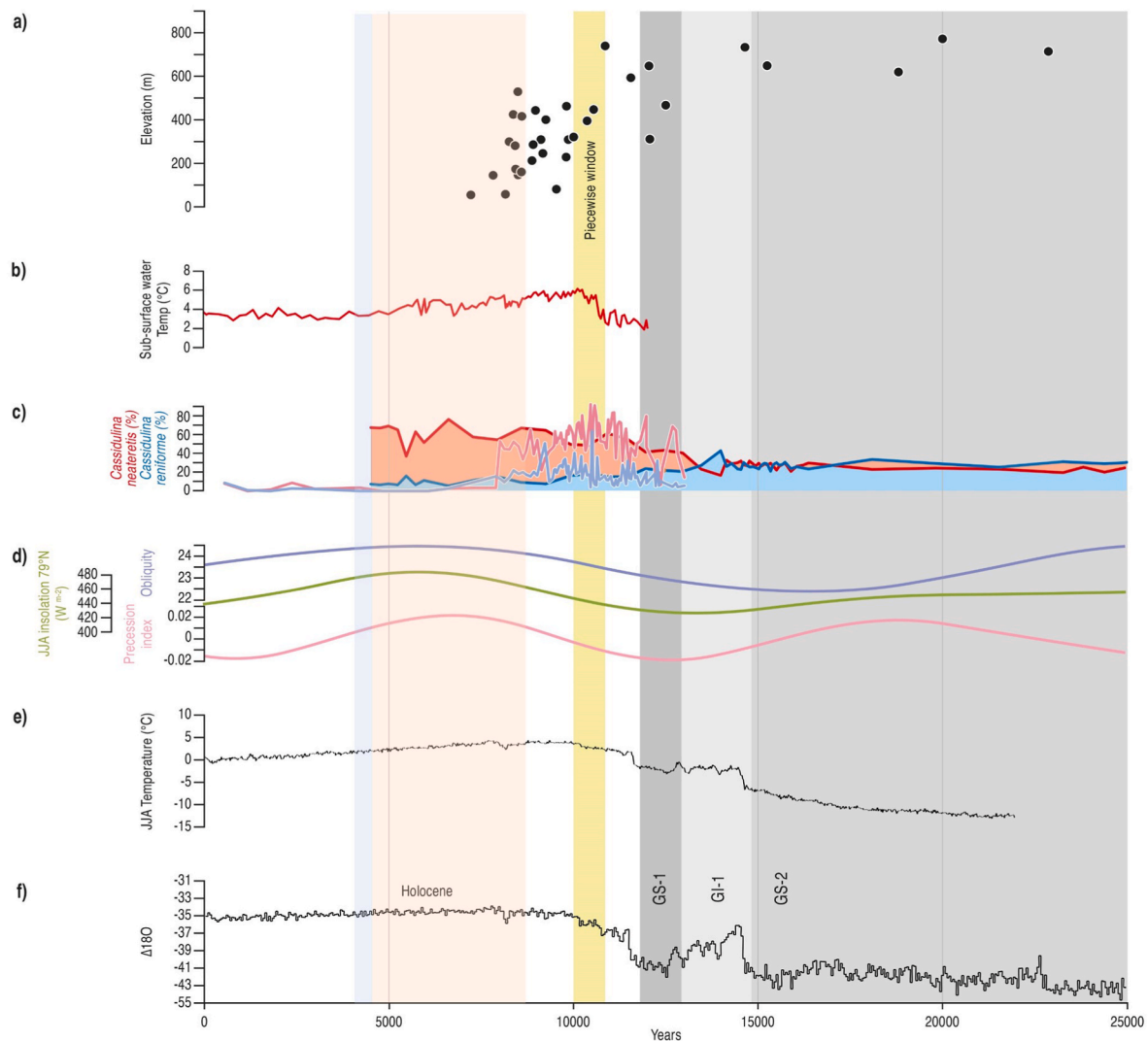
Fig. 11. a) The TCN dataset for Nioghalvfjerdsfjorden showing slow thinning and retreat between 23 and 10 ka and accelerated thinning and retreat post-10ka. Note the yellow piecewise regression window for the rapid deglaciation of Nioghalvfjerdsfjorden denoted by the orange bar (9.96–10.80 ka; 68% confidence). The pink bar represents open marine conditions/loss of ice shelf and blue bar the onset ice shelf reformation as recorded in Blåsø epishelf lake (Smith et al., 2023). b) Sub-surface ocean temperatures for the NE Greenland continental shelf based on Werner et al. (2016). c) Records of relative ocean warming and cooling based on the foraminifera records from the Fram Strait (Devendra et al., 2022; 4.5–25 ka) and the inner continental shelf adjacent to Nioghalvfjerdsfjorden (Davies et al., 2022; 0–12.5 ka). d) Orbital forcing (obliquity and precession) and Jun/July/August (JJA) insolation values for 79°N during deglaciation (Buizert et al., 2018). e) JJA air temperatures for 79°N during deglaciation (Buizert et al., 2018). f) The NGRIP δ18O record showing Greenland stadials GS-2 and GS-1 as well as Greenland Interstadial GI-1 (shaded grey zones).

from 10.9 to 10.1 ka cal BP. This overlaps closely with the increase in thinning and retreat rates identified in the piecewise regression (10.8–9.9 ka) and infers that ice was thinning rapidly along the Nioghalvfjerdsfjorden as it simultaneously withdrew from the continental shelf (Figs. 7 and 11). This coincided with maximum sub-surface ocean heat flux from AW ingress on to the inner continental shelf (Hansen et al., 2022; Davies et al., 2022; Lloyd et al., 2023), maximum JJA temperatures at 79°N and increasing insolation in the Early Holocene (Figs: 11 c, d, e, f).

From 10 ka onwards sub-surface ocean temperatures decreased, though JJA insolation and air temperatures continued to rise into the HTM. Larsen et al. (2018) also note the prominent role of precessional orbital forcing. These factors would have continued to drive high rates of ice stream surface lowering as air temperatures peaked at 2–4 °C higher than present. While surface lowering undoubtedly played a pivotal role in NEGIS retreat between 9.2 and 8.5 ka (when Nioghalvfjerdsfjorden deglaciated extremely quickly), the critical role of fjord bathymetry should also be considered. Nioghalvfjerdsfjorden has a steep reverse

bathymetric slope that reaches 900 m bsl close to Blåsø, the grounding line had unpinned from Bloch Nunatakker, and the ice stream had thinned through surface and submarine melt, as well as increased ice flux at the grounding line. All of which, would have pre-conditioned the ice stream for buoyant lift-off and marine ice sheet instability.

With contemporary thinning rates on NEGIS approaching 0.3–3.5 ma^{-1} due to a combination of grounding line retreat, ice shelf loss, surface ablation and dynamic upstream ice stream thinning (Khan et al., 2022), it is noteworthy that the contemporary and Early Holocene dynamic context of the ice stream are similar. Periods of sustained and accelerated atmospheric and ocean warming undoubtedly precondition ice streams for rapid retreat and thinning, but bathymetry remains a pivotal element in controlling ice dynamic feedbacks at present, and potentially in the past. During the Early Holocene in NE Greenland the role of ocean (2–6 °C) and atmospheric warming (2–4 °C) combined to drive high submarine and surface melt rates and concomitant thinning and, when coincident with a reverse submarine bed, this led to grounding line instability. Such conditions will define the dynamic

behaviour of the NEGIS over the next few decades, up to and beyond 2100AD.

5. Conclusions

The deglacial history of the NEGIS, and 79N Glacier in particular, has been reconstructed using TCN ages and the glacial geomorphology of the Nioghalvfjerdsfjorden region. High elevation terrain above ~900 m asl is characterised by autochthonous blockfield and the lack of correspondence between the ^{10}Be ages and the ^{26}Al ages points to a complex exposure/burial history. Coupled with the lack of glacially-moulded bedrock this indicates the presence of cold-based ice or long term periglacial conditions, or both, with minimal glacial erosion over extended time periods. During the early Quaternary plateau erosion rates were likely to be low, but from MIS16 -12 onwards enhanced glacial erosion led to fjord incision.The establishment of major marine terminating outlets such as ZI and 79N Glacier may relate to the onset of this period of incision. From 900 to 600 m asl allochthonous blockfield, bedrock surfaces and erratic evidence suggests a transitional glacial thermal regime such that below 600 m asl Nioghalvfjerdsfjorden exhibits a geomorphological signature of a warm-based ice stream. This operated prior to and during the last glacial cycle, with glacially abraded terrain, moraines and deltas providing evidence of ice stream advance, retreat and thinning.

Paired ^{10}Be/^{26}Al ages of 22.9 and 22.5 ka provide the best constraint on initial thinning in the outer fjord and over the coastal mountains. Both the geomorphic and geochronological evidence suggest ice warm-based ice at elevations between 700 and 800 m asl which would infer ice reached the outer continental shelf at the LGM. As deglaciation began and the grounding line retreated from the continental shelf edge concomitant thinning occurred inland. A clear geomorphic signal of ice stream surface thinning is manifested in nested lateral moraines and delta staircases which infer quasi-ice marginal stability during a punctuated initial deglaciation. Between 23 and 10ka thinning and retreat rates were slow through the fjord but post-10 ka it is evident that the coast and Nioghalvfjerdsfjorden deglaciated extremely quickly with complete fjord deglaciation below 500 m asl occurring between 10.0 and 8.5 ka. There can be little doubt that in the period between 12.0 and 10.0 ka both increasing air and ocean temperatures thinned the ice stream via surface and submarine melt. In addition, ice shelf loss by this point may have enhanced dynamic thinning (Syring et al., 2020; Lloyd et al., 2023). However, the final withdrawal of ice through Nioghalvfjerdsfjorden was likely facilitated by the action of marine ice sheet instability on a reverse bed.

It is possible that thinning and retreat rates reached a maximum of 5.29 ma^{-1} and 613 ma^{-1} respectively as the glacier withdrew west of Blåsø. Such estimates would place the Early Holocene collapse of NEGIS at the upper bounds of contemporary thinning and retreat rates seen both in Greenland and Antarctica. This would suggest that under warming scenarios analogous to the onset of the Holocene (air temperature: 2–4 °C; ocean 2–6 °C), NEGIS is likely to witness large scale dynamic changes on sub-centennial timescales.

Author contributions

D.H.R: NEGIS Project PI, Study Conceptualization and design, Field data collection, Data Analysis, Principal writer and reviewer; T.P.L, R.S. J, M.J.B, C.M.D, J.A.S, S.S.R.J, B.R.R: NEGIS onshore CO-I's and project team members who helped to collect, analyse and interpret the field data and review and critically revise the paper. A.R, D.F, D.G, A.D cosmogenic radionuclide laboratory sample analysis and age calculation. C.O, J.M.L, S.L.C and A.H: NEGIS offshore team and project partners. All authors approved the final version of the article.

Declaration of competing interest

The authors declare that they have no known competing financial interests or personal relationships that could have appeared to influence the work reported in this paper.

Data availability

Data is provided in the tables in the manuscript and in the supplementary material with respect to the NUNAIT model script and outlier calculations.

Acknowledgements

Appendix A. Supplementary data

Supplementary data to this article can be found online at https://doi.org/10.1016/j.quascirev.2024.108770.

References

An, L., Rignot, E., Wood, M., Willis, J.K., Mouginot, J., Khan, S.A., 2021. Ocean melting of the Zachariaeæ isstrøm and Nioghalvfjerdsfjorden glaciers, northeast Greenland. Proc. Natl. Acad. Sci. USA 118 (2), e2015483118.

Arndt, J.E., Jokat, W., Dorschel, B., Myklebust, R., Dowdeswell, J.A., Evans, J., 2015. A new bathymetry of the Northeast Greenland continental shelf: constraints on glacial and other processes. G-cubed 16 (10), 3733–3753.

Arndt, J.E., Jokat, W., Dorschel, B., 2017. The last glaciation and deglaciation of the Northeast Greenland continental shelf revealed by hydro-acoustic data. Quat. Sci. Rev. 160, 45–56.

Aschwanden, A., Fahnestock, M.A., Truffer, M., Brinkerhoff, D.J., Hock, R., Khroulev, C., Mottram, R., Khan, S.A., 2019. Contribution of the Greenland Ice Sheet to sea level over the next millennium. Sci. Adv. 5 (6), eaav9396.

Balco, G., 2020. Glacier change and paleoclimate applications of cosmogenic-nuclide exposure dating. Annu. Rev. Earth Planet Sci. 48, 21–48.

Ballantyne, C.K., 2018. Quaternary evolution and ice sheet history of contrasting landscapes in Uummannaq and Sukkertoppen. Quat. Sci. Rev. 149, 248–258.

Beel, C.R., Lifton, N.A., Briner, J.P., Goehring, B.M., 2016. Quaternary evolution and ice sheet history of contrasting landscapes in Uummannaq and Sukkertoppen, western Greenland. Quaternary Science Reviews 149, 248–258.

Bennike, O., Weidick, A., 2001. Late quaternary history around Nioghalvfjerdsfjorden and Jokelbugten, north-east Greenland. Boreas 30 (3), 205–227.

Bentley, M.J., Smith, J.A., Jamieson, S.S.R., Lindeman, M.R., Rea, B.R., Humbert, A., Lane, T., Darvill, C.M., Lloyd, J.M., Straneo, F., Helm, V., Roberts, D.H., 2023. Direct measurement of warm Atlantic intermediate water close to the grounding line of Nioghalvfjerdsfjorden (79N) glacier, north-East Greenland. Cryosphere 17 (5), 1821–1837.

Briner, J.P., Lifton, N.A., Miller, G.H., Refsnider, K., Anderson, R., Finkel, R., 2014. Using in situ cosmogenic ^{10}Be, ^{14}C, and ^{26}Al to decipher the history of polythermal ice sheets on Baffin Island, Arctic Canada. Quat. Geochronol. 19, 4–13.

Buizert, C., Keisling, B.A., Box, J.E., He, F., Carlson, A.E., Sinclair, G., DeConto, R.M., 2018. Greenland-wide seasonal temperatures during the last deglaciation. Geophys. Res. Lett. 45 (4), 1905–1914.

Choi, Y., Morlighem, M., Rignot, E., Mouginot, J., Wood, M., 2017. Modeling the response of Nioghalvfjerdsfjorden and Zachariæ isstrøm glaciers, Greenland, to ocean forcing over the next century. Geophys. Res. Lett. 44 (21), 11071–11079.

Dahl-Jensen, D., Mosegaard, K., Gundestrup, N., Clow, G.D., Johnsen, S.J., Hansen, A.W., Balling, N., 1998. Past temperatures directly from the Greenland ice sheet. Science 282 (5387), 268–271.

Davies, J., Mathiasen, A.M., Kristiansen, K., Hansen, K.E., Wacker, L., Alstrup, A.K.O., Munk, O.L., Pearce, C., Seidenkrantz, M.-S., 2022. Linkages between ocean circulation and the Northeast Greenland ice stream in the Early Holocene. Quat. Sci. Rev. 286, 107530.

Devendra, D., Łącka, M., Telesiński, M.M., Rasmussen, T.L., Sztybor, K., Zajączkowski, M., 2022. Paleoceanography of the northwestern Greenland sea and return Atlantic current evolution, 35–4 kyr BP. Global Planet. Change 217, 103947.

Evans, J., Ó Cofaigh, C., Dowdeswell, J.A., Wadhams, P., 2009. Marine geophysical evidence for former expansion and flow of the Greenland ice sheet across the north-East Greenland continental shelf. J. Quat. Sci. 24 (3), 279–293.

Fahnestock, M., Bindschadler, R., Kwok, R., Jezek, K., 1993. Greenland ice sheet surface properties and ice dynamics from ERS-1 SAR imagery. Science 262 (5139), 1530–1534.

Franke, S., Bons, P.D., Westhoff, J., Weikusat, I., Binder, T., Streng, K., Steinhage, D., Helm, V., Eisen, O., Paden, J.D., Eagles, G., Jansen, D., 2022. Holocene ice-stream shutdown and drainage basin reconfiguration in northeast Greenland. Nat. Geosci. 15 (12), 995–1001.

Gardner, A.S., Fahnestock, M.A., Agram, P.S., Scambos, T., Nilsson, J., Paolo, F.S., Walker, C.C., Meyer, F.J., Dehecq, A., 2018 December. ITS_LIVE: A new NASA MEaSUReS initiative to track the movement of the world's ice. AGU Fall Meeting Abstracts 2018, C14A, 02B.

Gardner, A.S., Fahnestock, M.A. and Scambos, T.A., 2019. ITS_LIVE Regional Glacier and Ice Sheet Surface Velocities, National Snow and Ice Data Center [data set].

Goelzer, H., Nowicki, S., Payne, A., Larour, E., Seroussi, H., Lipscomb, W.H., Gregory, J., Abe-Ouchi, A., Shepherd, A., Simon, E., Agosta, C., 2020. The future sea-level contribution of the Greenland ice sheet: a multi-model ensemble study of ISMIP6. Cryosphere 14 (9), 3071–3096.

Hansen, K.E., Lorenzen, J., Davies, J., Wacker, L., Pearce, C., Seidenkrantz, M.S., 2022. Deglacial to Mid Holocene environmental conditions on the northeastern Greenland shelf, western Fram Strait. Quat. Sci. Rev. 293, 107704.

Jakobsson, M., Mayer, L.A., Bringensparr, C., Castro, C.F., Mohammad, R., Johnson, P., Ketter, T., Accettella, D., Amblas, D., An, L., Arndt, J.E., 2020. The international bathymetric chart of the Arctic Ocean version 4.0. Scientific data 7 (1), 176.

Johnson, J.S., Bentley, M.J., Smith, J.A., Finkel, R., Rood, D., Gohl, K., Balco, G., Larter, R.D., Schaffer, J., 2014. Rapid thinning of pine island Glacier in the early Holocene. Science 343 (6174), 999–1001.

Jones, R.S., Mackintosh, A.N., Norton, K.P., Golledge, N.R., Fogwill, C.J., Kubik, P.W., Christl, M., Greenwood, S.L., 2015. Rapid Holocene thinning of an East Antarctic outlet glacier driven by marine ice sheet instability. Nature communications 6 (1), 8910.

Jones, R.S., Small, D., Cahill, N., Bentley, M.J., Whitehouse, P.L., 2019. iceTEA: tools for plotting and analysing cosmogenic-nuclide surface-exposure data from former ice margins. Quat. Geochronol. 51, 72–86.

Joughin, I., Smith, B.E., Howat, I.M., Scambos, T., Moon, T., 2010. Greenland flow variability from ice-sheet-wide velocity mapping. J. Glaciol. 56 (197), 415–430.

Khan, S.A., Kjær, K.H., Bevis, M., Bamber, J.L., Wahr, J., Kjeldsen, K.K., Bjørk, A.A., Korsgaard, N.J., Stearns, L.A., van den Broeke, M.R., Liu, L., Larsen, N.K., Muresan, I. S., 2014. Sustained mass loss of the northeast Greenland ice sheet triggered by regional warming. Nat. Clim. Change 4 (4), 292–299.

Khan, S.A., Choi, Y., Morlighem, M., Rignot, E., Helm, V., Humbert, A., Mouginot, J., Millan, R., Kjær, K.H., Bjørk, A.A., 2022. Extensive inland thinning and speed-up of northeast Greenland ice stream. Nature 611 (1937), 727–732.

Kjær, K.H., Bjørk, A.A., Kjeldsen, K.K., Hansen, E.S., Andresen, C.S., Siggaard-Andersen, M.L., Khan, S.A., Søndergaard, A.S., Colgan, W., Schomacker, A., Woodroffe, S., 2022. Glacier response to the little ice age during the neoglacial cooling in Greenland. Earth Sci. Rev. 227, 103984.

Klug, M., Schmidt, S., Bennike, O.L.E., Heiri, O., Melles, M., Wagner, B., 2009. Lake sediments from Store Koldewey, Northeast Greenland, as archive of Late Pleistocene and Holocene climatic and environmental changes. Boreas 38 (1), 59–71.

Knudsen, M.F., Egholm, D.L., Jacobsen, B.H., Larsen, N.K., Jansen, J.D., Andersen, J.L., Linge, H.C., 2015. A multi-nuclide approach to constrain landscape evolution and past erosion rates in previously glaciated terrains. Quat. Geochronol. 30, 100–113.

Konrad, H., Shepherd, A., Gilbert, L., Hogg, A.E., McMillan, M., Muir, A., Slater, T., 2018. Net retreat of Antarctic glacier grounding lines. Nat. Geosci. 11 (4), 258–262.

Krieger, L., Floricioiu, D., Neckel, N., 2019. Drainage Basin delineation for outlet glaciers of northeast Greenland based on Sentinel-1 ice velocities and TanDEM-X elevations. Rem. Sens. Environ. 237, 111483.

Lane, T.P., Roberts, D.H., Rea, B.R., Cofaigh, C.Ó., Vieli, A., Rodés, A., 2014. Controls upon the last glacial maximum deglaciation of the northern Uummannaq ice stream system, West Greenland. Quat. Sci. Rev. 92, 324–344.

Lane, T.P., Darvill, C.M., Rea, B.R., Bentley, M.J., Smith, J.A., Jamieson, S.S.R., Ó Cofaigh, C., Roberts, D.H., 2023. Geomorphological record of a former ice stream to ice shelf lateral transition zone in Northeast Greenland, Earth Surface Process. Landforms 48, 1321–1341.

Larsen, N.K., Levy, L.B., Carlson, A.E., Buizert, C., Olsen, J., Strunk, A., Bjork, A.A., Skov, D.S., 2018. Instability of the Northeast Greenland ice stream over the last 45,000 years. Nat. Commun. 9 (1), 1–8.

Lloyd, J.M., Park, L.A., Kuijpers, A., Moros, M., 2005. Early Holocene palaeoceanography and deglacial chronology of Disko Bugt, west Greenland. Quaternary Science Reviews 24 (14–15), 1741–1755.

Lloyd, J.M., Park, L.A., Kuijpers, A., Moros, M., 2006. Early Holocene palaeoceanography and deglacial chronology of Disko Bugt, west Greenland. Quat. Sci. Rev. 24 (14–15), 1741–1755.

Lloyd, J.M., Ribeiro, S., Weckström, K., Callard, L., Ó Cofaigh, C., Leng, M.J., Gulliver, P., Roberts, D.H., 2023. Ice-ocean interactions at the Northeast Greenland Ice stream (NEGIS) over the past 11,000 years. Quat. Sci. Rev. 308, 108068.

Long, A.J., Roberts, D.H., 2003. Late Weichselian deglacial history of Disko Bugt, west Greenland, and the dynamics of the Jakobshavns Isbræ ice stream. Boreas 32 (1), 208–226.

Mayer, C., Schaffer, J., Hattermann, T., Floricioiu, D., Krieger, L., Dodd, P.A., Kanzow, T., Licciulli, C., Schannwell, C., 2018. Large ice loss variability at Nioghalvfjerdsfjorden glacier, northeast-Greenland. Nat. Commun. 9 (1), 2768.

Mendelová, M., Hein, A.S., Rodés, Á., Xu, S., 2020. Extensive mountain glaciation in central Patagonia during marine isotope stage 5. Quat. Sci. Rev. 227, 105996.

Millan, R., Jager, E., Mouginot, J., Wood, M.H., Larsen, S.H., Mathiot, P., Jourdain, N.C., Bjørk, A., 2023. Rapid disintegration and weakening of ice shelves in North Greenland. Nat. Commun. 14 (1), 6914.

Moon, T., Fisher, M., Stafford, T., Harden, L., 2021, December. Integrating and exposing Greenland geospatial data via QGreenland. AGU Fall Meeting Abstracts (Vol. 2021, C55B–0589.

Morlighem, M., Williams, C.N., Rignot, E., An, L., Arndt, J.E., Bamber, J.L., Catania, G., Chauché, N., Dowdeswell, J.A., Dorschel, B., Fenty, I., 2017. BedMachine v3: complete bed topography and ocean bathymetry mapping of Greenland from multibeam echo sounding combined with mass conservation. Geophys. Res. Lett. 44 (21), 11–51.

Mouginot, J., Rignot, E., Scheuchl, B., Fenty, I., Khazendar, A., Morlighem, M., Buzzi, A., Paden, J., 2015. Fast retreat of Zachariæ isstrøm, northeast Greenland. Science 350 (6266), 1357–1361.

Müller, J., Werner, K., Stein, R., Fahl, K., Moros, M., Jansen, E., 2012. Holocene cooling culminates in sea ice oscillations in Fram Strait. Quat. Sci. Rev. 47, 1–14.

Nørgaard-Pedersen, N., Mikkelsen, N., Kristoffersen, Y., 2008. Late glacial and Holocene marine records from the independence Fjord and Wandel sea regions, North Greenland. Polar Res. 27 (2), 209–221.

Ó Cofaigh, C., Dowdeswell, J.A., Jennings, A.E., Hogan, K.A., Kilfeather, A., Hiemstra, J. F., Noormets, R., Evans, J., McCarthy, D.J., Andrews, J.T., Lloyd, J.M., 2013. An extensive and dynamic ice sheet on the West Greenland shelf during the last glacial cycle. Geology 41 (2), 219–222.

Pados-Dibattista, T., Pearce, C., Detlef, H., Bendtsen, J., Seidenkrantz, M.S., 2022. Holocene palaeoceanography of the Northeast Greenland shelf. Clim. Past 18 (1), 103–127.

Rasmussen, T.L., Pearce, C., Andresen, K.J., Nielsen, T., Seidenkrantz, M.S., 2022. Northeast Greenland: ice-free shelf edge at 79.4° N around the Last Glacial Maximum 25.5–17.5 ka. Boreas 51 (4), 759–775.

Rea, B.R., Whalley, W.B., Rainey, M.M., Gordon, J.E., 1996. Blockfields, old or new? Evidence and implications from some plateaus in northern Norway. Geomorphology 15 (2), 109–121.

Roberts, D.H., Long, A.J., Schnabel, C., Freeman, S., Simpson, M.J., 2008. The deglacial history of southeast sector of the Greenland ice sheet during the last glacial maximum. Quat. Sci. Rev. 27 (15–16), 1505–1516.

Roberts, D.H., Rea, B.R., Lane, T.P., Schnabel, C., Rodés, A., 2013. New constraints on Greenland ice sheet dynamics during the last glacial cycle: evidence from the Uummannaq ice stream system. Journal of Geophysical Research - Earth Surface 118 (2), 519–541.

Rodés, Á., 2021. The Nunatak ice thinning (NUNAIT) calculator for Cosmonuclide elevation profiles. Geosciences 11 (9), 362.

Schaffer, J., Kanzow, T., von Appen, W.-J., von Albedyll, L., Arndt, J.E., Roberts, D.H., 2020. Bathymetry constrains ocean heat supply to Greenland's largest glacier tongue. Nat. Geosci. 13 (3), 227–231.

Seroussi, H., Morlighem, M., Rignot, E., Khazendar, A., Larour, E., Mouginot, J., 2013. Dependence of century-scale projections of the Greenland ice sheet on its thermal regime. J. Glaciol. 59 (218), 1024–1034.

Shepherd, A., Ivins, E., Rignot, E., Smith, B., van den Broeke, M., Velicogna, I., Whitehouse, P., Briggs, K., Joughin, I., Krinner, G., Nowicki, S., Payne, T., Scambos, T., Schlegel, N., A, G., Agosta, C., Ahlstrøm, A., Babonis, G., Barletta, V.R., Bjørk, A.A., Blazquez, A., Bonin, J., Colgan, W., Csatho, B., Cullather, R., Engdahl, M. E., Felikson, D., Fettweis, X., Forsberg, R., Hogg, A.E., Gallee, H., Gardner, A., Gilbert, L., Gourmelen, N., Groh, A., Gunter, B., Hanna, E., Harig, C., Helm, V., Horvath, A., Horwath, M., Khan, S., Kjeldsen, K.K., Konrad, H., Langen, P.L., Lecavalier, B., Loomis, B., Luthcke, S., McMillan, M., Melini, D., Mernild, S., Mohajerani, Y., Moore, P., Mottram, R., Mouginot, J., Moyano, G., Muir, A., Nagler, T., Nield, G., Nilsson, J., Noël, B., Otosaka, I., Pattle, M.E., Peltier, W.R., Pie, N., Rietbroek, R., Rott, H., Sandberg Sørensen, L., Sasgen, I., Save, H., Scheuchl, B., Schrama, E., Schröder, L., Seo, K.-W., Simonsen, S.B., Slater, T., Spada, G., Sutterley, T., Talpe, M., Tarasov, L., van de Berg, W.J., van der Wal, W., van Wessem, M., Vishwakarma, B.D., Wiese, D., Wilton, D., Wagner, T., Wouters, B., Wuite, J., The, I.T., 2020. Mass balance of the Greenland ice sheet from 1992 to 2018. Nature 579 (7798), 233–239.

Skov, D.S., Andersen, J., Olsen, J., Jacobsen, B., Knudsen, M., Jansen, J., 2020. Constraints from cosmogenic nuclides on the glaciation and erosion history of dove Bugt, Northeast Greenland. GSA Bulletin 132 (11–12), 2282–2294.

Small, D., Bentley, M.J., Jones, R.S., Pittard, M.L., Whitehouse, P.L., 2019. Antarctic ice sheet palaeo-thinning rates from vertical transects of cosmogenic exposure ages. Quat. Sci. Rev. 206, 65–80.

Smith, M.P., Higgins, A.K., Soper, N.J., Sønderholm, M., 2004. The Neoproterozoic Rivieradal group of Kronprins Christian Land, eastern North Greenland. GEUS Bulletin 6, 29–39.

Smith, J.A., Callard, L., Bentley, M.J., Jamieson, S.S.R., Sánchez-Montes, M.L., Lane, T. P., Lloyd, J.M., McClymont, E.L., Darvill, C.M., Rea, B.R., O'Cofaigh, C., Gulliver, P., Ehrmann, W., Jones, R.S., Roberts, D.H., 2023. Holocene history of the 79° N ice shelf reconstructed from epishelf lake and uplifted glaciomarine sediments. Cryosphere 17 (3), 1247–1270.

Stein, R., Nam, S.-I., Grobe, H., Hubberten, H., 1996. Late Quaternary glacial history and short-term ice-rafted debris fluctuations along the East Greenland continental margin. Geological Society, London, Special Publications 111 (1), 135–151.

Stokes, C.R., Abram, N.J., Bentley, M.J., Edwards, T.L., England, M.H., Foppert, A., Jamieson, S.S., Jones, R.S., King, M.A., Lenaerts, J.T., Medley, B., 2022. Response of the East Antarctic Ice Sheet to past and future climate change. Nature 608 (7922), 275–286.

Straneo, F., Heimbach, P., 2013. North Atlantic warming and the retreat of Greenland's outlet glaciers. Nature 504 (7478), 36–43.

Strunk, A., Knudsen, M.F., Egholm, D.L., Jansen, J.D., Levy, L.B., Jacobsen, B.H., 2017. One million years of glaciation and denudation history in West Greenland. Nat. Commun. 8 (1), 1–8.

Sugden, D., 1974. Landscapes of Glacial Erosion in Greenland and Their Relationship to Ice, Topographic and Bedrock Conditions, vol. 7. Institute of British Geographers Special Publication, pp. 177–195.

Syring, N., Lloyd, J.M., Stein, R., Fahl, K., Roberts, D.H., Callard, L., O'Cofaigh, C., 2020. Holocene interactions between glacier retreat, sea ice formation, and Atlantic water advection at the inner northeast Greenland continental shelf. Paleoceanogr. Paleoclimatol. 35 (11), e2020PA004019.

Vinther, B.M., Buchardt, S.L., Clausen, H.B., Dahl-Jensen, D., Johnsen, S.J., Fisher, D.A., Koerner, R.M., Raynaud, D., Lipenkov, V., Andersen, K.K., Blunier, T., 2009. Holocene thinning of the Greenland ice sheet. Nature 461 (7262), 385–388.

Werner, K., Müller, J., Husum, K., Spielhagen, R.F., Kandiano, E.S., Polyak, L., 2016. Holocene sea subsurface and surface water masses in the Fram Strait – comparisons of temperature and sea-ice reconstructions. Quat. Sci. Rev. 147, 194–209.

Wilson, N.J., Straneo, F., 2015. Water exchange between the continental shelf and the cavity beneath Nioghalvfjerdsbræ (79 North Glacier). Geophys. Res. Lett. 42 (18), 7648–7654.

Winkelmann, D., Jokat, W., Jensen, L., Schenke, H.-W., 2010. Submarine end moraines on the continental shelf off NE Greenland – implications for Lateglacial dynamics. Quat. Sci. Rev. 29 (9–10), 1069–1077.

Xu, S., Dougans, A.B., Freeman, S.P., Schnabel, C., Wilcken, K.M., 2010. Improved ^{10}Be and ^{26}Al AMS with a 5 MV spectrometer. Nucl. Instrum. Methods Phys. Res. Sect. B Beam Interact. Mater. Atoms 268 (7–8), 736–738.

Young, N.E., Briner, J.P., Axford, Y., Csatho, B., Babonis, G.S., Rood, D.H., Finkel, R.C., 2011. Response of a marine-terminating Greenland outlet glacier to abrupt cooling 8200 and 9300 years ago. Geophys. Res. Lett. 38 (24), L24701.

Young, N.E., Schaefer, J.M., Briner, J.P., Goehring, B.M., 2013. A 10 Be production-rate calibration for the Arctic. J. Quat. Sci. 28 (5), 515–526.

Zeising, O., Neckel, N., Dörr, N., Helm, V., Steinhage, D., Timmermann, R., Humbert, A., 2023. Extreme Melting at Greenland's Largest Floating Ice Tongue. EGUsphere, pp. 1–35.